Huntingtin Aggregation Kinetics and Their Pathological Role in a Drosophila Huntington's Disease Model

Citation: Weiss, K. R., Y. Kimura, W.-C. M. Lee, and J. T. Littleton. "Huntingtin Aggregation Kinetics and Their Pathological Role in a Drosophila Huntington's Disease Model." Genetics 190, no. 2 (February 1, 2012): 581–600.

As Published: http://dx.doi.org/10.1534/genetics.111.133710

Publisher: Genetics Society of America, The

Persistent URL: http://hdl.handle.net/1721.1/85583

Version: Author's final manuscript: final author's manuscript post peer review, without publisher's formatting or copy editing

Huntingtin Aggregation Kinetics and their Pathological Role in a *Drosophila* Huntington's Disease Model

Kurt R. Weiss[*], Yoko Kimura[*,§], Wyan-Ching Mimi Lee[*] and J. Troy Littleton[*,1]

[*]The Picower Institute for Learning and Memory, Department of Biology and Department of Brain and Cognitive Sciences, Massachusetts Institute of Technology, Cambridge, MA 02139

[§]Laboratory of Protein Metabolism, The Tokyo Metropolitan Institute of Medical Science, Kamikitazawa, Setagaya-Ku, Tokyo 156-8506, Japan

Running Title: Analysis of Huntington Aggregation Kinetics and Toxicity

[1]Corresponding author: The Picower Institute for Learning and Memory, 43 Vassar St., 46-3243, Cambridge, MA 02139. Tel: 617-452-2605. E-mail: troy@mit.edu

Key Words: Huntingtin, Polyglutamine, Neurodegeneration, *Drosophila*, Axonal Transport, Aggregation

Abstract

Huntington's Disease is a neurodegenerative disorder resulting from expansion of a polyglutamine tract in the Huntingtin protein. Mutant Huntingtin forms intracellular aggregates within neurons, though it is unclear if aggregates or more soluble forms of the protein represent the pathogenic species. To examine the link between aggregation and neurodegeneration, we generated *Drosophila melanogaster* transgenic strains expressing fluorescently-tagged human *huntingtin* encoding pathogenic (Q138) or non-pathogenic (Q15) proteins, allowing *in vivo* imaging of Huntingtin expression and aggregation in live animals. Neuronal expression of pathogenic Huntingtin leads to pharate adult lethality, accompanied by formation of large aggregates within the cytoplasm of neuronal cell bodies and neurites. Live imaging and FRAP analysis of pathogenic Huntingtin demonstrated that new aggregates can form in neurons within 12 hours, while pre-existing aggregates rapidly accumulate new Huntingtin protein within minutes. To examine the role of aggregates in pathology, we conducted haplo-insufficiency suppressor screens for Huntingtin-Q138 aggregation or Huntingtin-Q138-induced lethality using deficiencies covering ~80% of the *Drosophila* genome. We identified two classes of interacting suppressors in our screen: those that rescue viability while decreasing Huntingtin expression and aggregation, and those that rescue viability without disrupting Huntingtin aggregation. The most robust suppressors reduced both soluble and aggregated Huntingtin levels, suggesting toxicity is likely to be associated with both forms of the mutant protein in Huntington's Disease.

Introduction

Huntington's disease (HD) is an autosomal dominant neurodegenerative disorder and one of the first characterized members of a family of neurological diseases that result from expansion of a polyglutamine (polyQ) tract within the causative protein (ORR and ZOGHBI 2007). HD is characterized by neurodegeneration and formation of neuronal intracellular inclusions, primarily in the striatum and cortex, leading to motor impairment, personality disorders, dementia and ultimately death (PORTERA-CAILLIAU *et al*. 1995; VONSATTEL *et al*. 1985). Currently, HD has no known cure and treatments focus on delaying HD-associated symptoms. The causative mutation in HD is expansion of a CAG tract beyond 35 repeats in exon 1 of the *IT15* gene encoding Huntingtin (Htt) (HUNTINGTON'S DISEASE RESEARCH COLLABORATION, 1993). Similar to other polyQ-repeat neurological disorders, abnormal protein conformation(s) secondary to polyQ expansion are central to HD pathogenesis (PERSICHETTI *et al*. 1999; SCHERZINGER *et al*. 1997). The expanded polyQ Htt protein can exist in multiple states (HOFFNER *et al*. 2005; NAGAI *et al*. 2007), including aberrantly folded monomeric forms, oligomeric micro-aggregates, fibril states and larger inclusion body aggregates. It is currently unclear which form(s) of mutant Htt are pathogenic and how the abnormally folded protein causes neuronal toxicity.

PolyQ expansion leading to aggregation is a common theme in neurodegenerative disorders. Spinocerebellar ataxias (SCA1 SCA2, SCA3/MJD, SCA6, SCA7, SCA17), spinal bulbar muscular atrophy (SMBA), and dentatorubral pallidoluysian atrophy (DRPLA) all involve polyQ expansion, aggregation, and neurodegeneration (KIMURA *et al*. 2007). Evidence that aggregates are toxic is mostly correlative for these diseases, but several studies support the aggregation-toxicity hypothesis. The threshold of polyQ repeat number required for *in vitro* aggregation threshold is similar to that required for disease manifestation (DAVIES *et al*. 1997;

SCHERZINGER *et al*. 1999). Longer polyQ tracts have faster *in vitro* aggregation kinetics and result in earlier disease onset (SCHERZINGER *et al*. 1999). Similarly, treatments that suppress aggregation, including chaperone overexpression (CARMICHAEL *et al*. 2000) and administration of small molecule aggregation inhibitors (CHOPRA *et al*. 2007), have been shown to decrease neurodegeneration. Live imaging demonstrates that Htt aggregates can sequester and alter kinetics of trafficked organelles and proteins such as synaptic vesicles (SINADINOS *et al*. 2009) and transcription factors (CHAI *et al*. 2002). However, there is also evidence that aggregates may be inert or even neuroprotective. Medium spiny projection neurons of the striatum exhibit fewer Htt aggregates than striatal interneurons, yet are more vulnerable to neurodegeneration in HD (KUEMMERLE *et al*. 1999). Additionally, several mouse (HODGSON *et al*. 1999) and *Drosophila* (ROMERO *et al*. 2008) HD models expressing full-length mutant Htt show selective neurodegeneration and behavioral phenotypes without obvious aggregation. Conversely, the HD mouse model "short-stop" expresses an N-terminal polyQ-Htt fragment and displays aggregate formation, but no neuronal dysfunction or degeneration (SLOW *et al*. 2005). Indeed, neuronal cell death associated with transient expression of mutant Htt in cultured striatal neurons is inversely proportional to Htt aggregate formation (ARRASATE *et al*. 2004), suggesting that inclusion body formation may decrease levels of other toxic forms of Htt and promote neuronal survival. There is also evidence suggesting that oligomers precede aggregate formation and are the toxic species in HD (LAJOIE and SNAPP 2010; LAM *et al*. 2008). These contradictory results in different cellular contexts and HD models have led to confusion over the toxicity of aggregates, and subsequently, over whether therapeutic approaches in HD should focus on reducing or enhancing aggregate formation.

To further analyze the link between aggregation and toxicity in a model system, we generated transgenic *Drosophila* that express an N-terminal fragment of the human Htt gene with either a pathogenic polyQ tract of 138 repeats (HttQ138), corresponding to a juvenile form of HD, or a wild-type non-pathogenic tract of 15 repeats (HttQ15). The Htt transgene used in our analysis is a human Caspase-6 cleavage fragment containing exons 1 to 12 of the larger Htt locus. Proteolysis of Htt at the Caspase-6 site is an important pathogenic event in HD (GRAHAM *et al*. 2006). Given the uncertainty of cleavage of a larger human Htt transgenic protein in *Drosophila*, the 588 aa fragment represents an attractive biologically relevant cleavage product. The constructs were fused to monomeric red fluorescent protein (mRFP) (CAMPBELL *et al*. 2002) or enhanced green fluorescent protein (eGFP) to allow *in vivo* analysis of aggregate formation and localization. Expression of pathogenic Htt leads to the formation of cytoplasmic aggregates and causes death during the pupal stage. This model provides a tractable system to analyze Htt aggregation kinetics in live animals and to conduct forward genetic screens for modifiers of HD pathology and/or aggregation, allowing us to examine the link between Htt aggregation and neuronal toxicity.

Materials and Methods

Generation of Htt Constructs: cDNAs for mRFP-HttQ15, mRFP-HttQ138, eGFP-HttQ15 and eGFP-HttQ138 were subcloned into EcoRI (blunt end ligation) and KpnI sites of the pUAST expression vector. cDNA for eGFP-HttQ138-mRFP was subcloned into the XbaI site of the pUAST vector. HttQ15 and HttQ138 cDNAs were kindly provided by Ray Truant (Department of Biochemistry, McMaster University). cDNA for HttQ96-GFP was kindly provided by David Housman (Center for Cancer Research, MIT) and subcloned into the KpnI and XbaI sites of the pUAST vector. Microinjection of constructs was performed by Genetics Services (Cambridge, MA).

S2 Cell Transfection and Analysis: cDNAs for mRFP-HttQ15 and mRFP-HttQ138 were subcloned into the BamH1 and EcoRI (blunt end ligation) sites of the pSR11 S2 transformation vector. To generate constructs expressing mRFP-HttQ15-eGFP and mRFP-HttQ138-eGFP, mRFP-HttQ15 and mRFP-HttQ138 cDNAs were PCR amplified with a forward primer containing an EcoRI restriction site and a reverse primer containing a 3' Sal I site and subcloned into the pPL17 vector. Constructs were transfected with 50 μL cytofectene (BioRad) into *Drosophila* S2 cells using the BioRad Liposome Mediated Transfection Protocol. After 72 hours, 20 μL cell suspensions were fixed with 3.7% formaldehyde in PBT and mounted on slides with 50% glycerol. Images were captured with a Zeiss Pascal laser scanning confocal microscope (Carl Zeiss MicroImaging, Inc.) using the accompanying Zeiss PASCAL software.

Glue Secretion Assay: Pupae reared at 25ºC were isolated shortly after pupariation and placed

on slides with the ventral side facing up using double-sided tape. Visualization was performed on a Pascal confocal microscope (Zeiss).

***Drosophila* Genetics and Deficiency Screen:** *Drosophila* were maintained on standard medium at 25ºC. The deficiency collection used in the screen was obtained from the Bloomington Stock Center. Males from deficiency lines on chromosomes II and III were crossed to C155; A37/CyO-GFP or C155; *Df(3)3450*/TM6 virgins, respectively. For the viability screen, F1 C155/y; Df/Balancer males were mated to homozygous mRFP-HttQ138 high expression females and the number of F2 males and females was scored. For the aggregation screen, F1 C155/y; Df/Balancer males were mated to homozygous mRFP-HttQ138 low expression virgins and live wandering 3rd instar larvae expressing mRFP-HttQ138/Df were viewed under a fluorescent stereoscope (Zeiss) to assay changes in aggregation in larval salivary glands. For aggregation formation analysis, the *CCAP*-Gal4 driver was recombined with a *tubulin*-Gal80^{ts} repressor to drive high expression mRFP-HttQ138 in a temporally restricted manner. mRFP-HttQ138 expression was repressed at 19°C until the 2nd instar stage, at which point larvae were moved to 30°C to induce expression.

Adult Viability Analysis*: Drosophila* viability assays were performed on white/C155, HttQ96-GFP/C155, mRFP-HttQ15/C155, mRFP-HttQ138/C155, and mRFP-HttQ138B/C155 flies by daily quantification of lethality for 100 females of each genotype. Flies were aged at 25ºC, with 20 flies per vial, and transferred every 2-3 days.

Western Blot Analysis*:* For HttQ96-GFP Western blots, *Drosophila* were frozen in liquid nitrogen and vortexed. 20 heads for each indicated genotype were isolated and homogenized in sample buffer, and proteins were separated on 10% SDS-PAGE gels and transferred to nitrocellulose. Blots were incubated with rabbit anti-GFP sc8334 (Santa Cruz Biotechnology) at 1:1000. For eGFP-HttQ138/Q15 and mRFP-HttQ138/Q15, five larvae for each genotype were homogenized in sample buffer and proteins were separated on 10% SDS-PAGE gels. Blots were incubated with mouse anti-Htt MAb2166 (Chemicon) at 1:1000 or anti-Actin (JLA20 antisera, Developmental Studies Hybridoma Bank) at 1:1000. To assay for cleavage of Htt *in vivo*, we crossed UAS-HttQ138-mRFP and UAS-eGFP-HttQ138-mRFP to C155 GAL4 driver strains and prepared head extracts from F1 progeny expressing Htt. One head extract per lane was loaded and blots were probed with anti-Htt antibodies. Western blots were visualized on a Li-Cor Odyssey infrared imaging system and protein expression quantified with the accompanying software.

Immunostaining: Wandering 3rd instar larvae reared at 25ºC were dissected as previously described (RIECKHOF *et al*. 2003), except that fixation was limited to 10 minutes in 4% formaldehyde. Images were captured with a Zeiss Pascal laser scanning confocal microscope (Carl Zeiss MicroImaging, Inc.) using the accompanying Zeiss PASCAL software.

Quantitative RT-PCR: Quantitative RT-PCR was carried out using an Applied Biosystems 7300 Real-Time PCR System. Total RNA was extracted from 10-15 adult flies per sample using an RNeasyMini Kit (Qiagen) and treated with DNase I (Ambion) according to the manufacturers' instructions. Single stranded cDNA was synthesized in a total volume of 20 μL

from 1 μg of total RNA using a High Capacity cDNA Reverse Transcription Kit (Applied Biosystems) according to the manufacturer's protocol. PCR was carried out in triplicate for each of two independent total RNA samples per genotype in optical 96-well plates (Applied Biosystems). The reaction mixtures were as follows: 25 μL of 2x QuantiTect SYBR Green PCR Master Mix (Qiagen), 300 nM forward primer, 300 nM reverse primer, and 5 μL of single stranded cDNA (see above) in a total volume of 50 μL. A final dissociation step was carried out to evaluate product integrity, and reaction samples were run on a 1.2% agarose gel and stained with ethidium bromide. The primer sequences were as follows: Act88F (actin) forward 5'-ACTTCTGCTGGAAGGTGGAC-3' and reverse 5'-ATCCGCAAGGATCTGTATGC-3'.

FRAP and Live Imaging: FRAP analysis was carried out using a Zeiss spinning disk confocal microscope with Perkin Elmer Velocity 4-D imaging software. Animals were anesthetized with Suprane in a custom chamber that allows imaging through the cuticle of a live 3rd instar larvae (FUGER *et al*. 2007) with a 63X oil objective. Camera settings were adjusted so that the aggregate to be bleached was just below saturation. Aggregates were photobleached using 100% laser power at 546 nm for two to five iterations through the entire z-plane until they were at 35% of the original fluorescence intensity. Z-stack recovery images were recorded at a rate of one per minute for 60 minutes for FRAP recovery curves at long time scales. An imaging rate of one frame per 10 seconds was used for analysis of how individual puncta interact with aggregates and for characterizing aggregate formation events.

Results

A 588 amino acid N-terminal fragment of pathogenic human Htt reduces *Drosophila* lifespan: To explore pathogenic mechanisms in HD, we generated transgenic *Drosophila* that express 588 aa N-terminal fragments of human Htt with either a pathogenic polyQ tract of 138 repeats (HttQ138) or a non-pathogenic tract of 15 repeats (HttQ15). While several models of HD have focused on expression of the polyQ-containing first exon of Htt alone, the 588 amino acid fragment is truncated near a number of well-characterized caspase cleavage sites important in the generation of aggregate-forming Htt fragments (GRAHAM *et al*. 2006; KIM *et al*. 2001; WELLINGTON *et al*. 2002). Additionally, many sites of protein interaction that are lost in exon 1 constructs are conserved in the longer 588 aa fragment, including a region of well-conserved HEAT repeats thought to be involved in Htt binding to interaction partners such as HIP1, HAP1, and HIP14 (HARJES and WANKER 2003). Htt was fluorescently tagged with mRFP or eGFP at the N-terminus, or tagged at both ends with eGFP at the N-terminus and mRFP at the C-terminus (Figure 1A). For comparison, we generated a transgenic strain expressing exon 1 (81 aa) of the human Htt protein with a pathogenic 96Q repeat, fused to GFP at the C-terminus (HttQ96-GFP). All constructs were expressed using the UAS-GAL4 system, allowing for temporal and tissue-specific control of transgene expression. To confirm transgene expression, strains were crossed to the neuronal driver *elav*-GAL4 (C155), and Htt expression in offspring was assessed through Western blot analysis with anti-human Htt antibodies (Figure 1B). No Htt expression is detected in control *white* strains crossed to C155, while mRFP-Htt, eGFP-Htt, and HttQ96-GFP lines all demonstrate abundant Htt expression. As expected, the product detected in HttQ15 strains lacking the expanded polyQ tract is smaller than that in HttQ138 or HttQ96 strains. These

transgenic lines allow imaging of Htt aggregation in live *Drosophila*, providing a resource for following Htt dynamics *in vivo*.

To determine the effects of pathogenic and non-pathogenic Htt expression in *Drosophila*, viability profiles were generated for control and HttQ138-expressing animals. Pan-neuronal expression of mRFP-HttQ138 with C155 causes pharate adult lethality with less than 1% viable adult escapers. Expression of pathogenic Htt with a weaker *elav*-GAL4 driver results in viable adults that appear behaviorally normal at the time of eclosion. However, several days after eclosion, these adults begin to exhibit motor coordination defects and abnormal grooming behaviors, worsening with age and resulting in premature death. Similar defects occur at a later time in a separate mRFP-HttQ138 insertion line (mRFP-HttQ138B) expressing pathogenic Htt at a lower level, as well as in flies expressing the pathogenic HttQ96-GFP exon 1 protein (Figure 1C). These behaviors are not observed in mRFP-HttQ15-expressing or control *Drosophila*. To quantify the reduction in viability of pathogenic Htt-expressing lines, lifespan curves were generated for control adults and adults expressing mRFP-HttQ15, mRFP-HttQ138, mRFP-HttQ138B or HttQ96-GFP (Figure 1C). The T_{50} (age at which 50% of the culture has died) for mRFP-HttQ138 lines is dramatically decreased by over 70% in comparison to controls. mRFP-HttQ138B expression results in a 30% decrease in T_{50}, indicating that lethality is correlated with the level of expression of the pathogenic protein. HttQ96-GFP lines also demonstrate a decrease in T_{50} of 50%, suggesting that expression of the expanded polyQ-containing first exon of Htt is also toxic. Decreases in T_{50} for all lines expressing fragments of the pathogenic Htt protein, but not the normal protein, indicate that expression of pathogenic Htt results in behavioral dysfunction and reduced lifespan in *Drosophila*. Although differences in genetic background

may contribute to some of the effects on lifespan, polyQ expansion in Htt consistently reduces lifespan in our analysis.

Pathogenic Htt forms cytoplasmic aggregates in neuronal and non-neuronal cells *in vivo:* A hallmark of HD is the formation of intracellular aggregates immunopositive for the pathogenic Htt protein. Aggregates have been found in the nucleus, cell body and neurites in HD (DIFIGLIA *et al*. 1997). However, it is unknown whether toxic Htt activity occurs in the nucleus, in the cytoplasm, or in both. To determine the intracellular distribution of our pathogenic and non-pathogenic transgenic Htt fragments, *Drosophila* S2 cells were transiently transfected with the mRFP-HttQ15 or mRFP-HttQ138 constructs and fixed cells were imaged by confocal microscopy. While mRFP-HttQ15 demonstrated diffuse cytoplasmic localization, mRFP-HttQ138 formed large, distinct cytoplasmic aggregates (Figure 2A). Neither protein localized to the nucleus.

To assess whether intracellular aggregates are formed *in vivo* by transgenic Htt proteins in *Drosophila*, UAS-mRFP-Htt strains were crossed to lines expressing the *elav*-GAL4 driver. As observed in S2 cells, the non-pathogenic mRFP-HttQ15 remained diffuse throughout the cytoplasm and neurites of neurons in both the CNS (Figure 2B) and PNS (Figure 2D). In contrast, distinct Htt aggregates were observed throughout the cytoplasm and neurites in lines expressing the pathogenic mRFP-HttQ138 (Figure 2C, E). To observe subcellular localization in other cell types, mRFP-HttQ15 and mRFP-HttQ138 were driven with a ubiquitous GAL4 driver (*tubulin*-GAL4). In non-neuronal cells, including epidermis (Figure 2F) and salivary glands (Figure 2H), mRFP-HttQ15 localized diffusely in the cytoplasm, while mRFP-HttQ138 formed cytoplasmic aggregates (Figure 2G & I). Nuclear aggregates were not observed in any cell type.

These results suggest that Htt fragments induce pathology primarily through a cytoplasmic localization in this *Drosophila* model.

Mutant Htt causes defects in salivary gland glue secretion in *Drosophila:* To determine whether HttQ138 expression might cause defects in non-neuronal tissues, we tested whether Htt expression in larval salivary glands causes cellular dysfunction. We analyzed secretion of the GFP-tagged salivary gland glue protein Sgs3 (BIYASHEVA *et al*. 2001) in controls and animals expressing mRFP-HttQ15 or mRFP-HttQ138 (Figure 3). During normal puparation, *Drosophila* secretes ecdysteriod-induced glue granules that mediate attachment of the developing pupal case to surfaces. While glue secretion is evident in both control and mRFP-HttQ15-expressing pupae (Figure 3A, B), secretion is decreased in pupae expressing mRFP-HttQ138 (Figure 3C). Normal 3rd instar larval salivary gland cells are filled with glue proteins (Figure 3D) that are depleted during pupariation (Figure 3E). In contrast, the pupal salivary glands of mRFP-HttQ138-expressing larvae retain glue (Figure 3G), suggesting salivary gland dysfunction mediated by the cytoplasmic accumulation of mutant Htt.

The 588 aa fragment of pathogenic human Htt does not produce nuclear cleavage products in *Drosophila:* Mutant forms of Htt have been reported to undergo cleavage by caspases and calpains to generate smaller N-terminal fragments that can be observed in the nucleus and cytoplasm (GAFNI *et al*. 2004; KIM *et al*. 2001; LUNKES *et al*. 2002; WELLINGTON *et al*. 2002). To determine whether cleavage of the N-terminal 588 aa of Htt occurs in our *Drosophila* model to generate smaller fragments that might localize to the nucleus, S2 cells were transiently transfected with 588 aa Htt constructs labeled with eGFP at the N-terminus and mRFP at the C-

terminus. Complete co-localization of the eGFP and mRFP signals was observed for both the normal eGFP-HttQ15-mRFP fragment (Figure 4A), and the pathogenic eGFP-HttQ138-mRFP fragment (Figure 4B). These results suggest that cleavage of Htt does not occur in the context of *Drosophila* S2 cells, or alternatively, that any cleaved N- and C-terminal fragments of Htt remain co-localized in the cytoplasm.

To assess whether cleavage and separation of N- and C-terminal fragments of Htt occur *in vivo*, we generated transgenic strains expressing the double-labeled pathogenic Htt fragment eGFP-HttQ138-mRFP. As observed in the S2 cell model, eGFP and mRFP signals co-localized in all tissues studied, including CNS neurons (Figure 4C), salivary gland cells (Figure 4D), and epidermal cells (Figure 4E), suggesting that pathogenic Htt is unlikely to be cleaved *in vivo* in *Drosophila*. Neither N- or C- terminal fragments of Htt are observed in the nucleus. To further test if cleavage occurs *in vivo*, we performed Western analysis with anti-Htt antibodies to probe for breakdown products that would result from cleavage of the protein. As shown in Figure 4F, no differential cleavage products were observed by Western analysis in head extracts prepared from animals expressing HttQ138-mRFP versus eGFP-HttQ138-mRFP animals. Thus, the pathogenic Htt-mediated toxicity seen in our *Drosophila* HD model does not appear to require Htt cleavage or nuclear entry, and reflects an effect of the 588 aa fragment in the cytoplasm.

Exon 1 of pathogenic Htt forms cytoplasmic and neuritic aggregates: Many classic HD models express exon 1 of the mutant protein (DAVIES *et al*. 1997; JACKSON *et al*. 1998; KROBITSCH and LINDQUIST 2000; TAGAWA *et al*. 2004), which is capable of forming inclusions postulated to play a role in HD pathology (BECHER *et al*. 1998; DAVIES *et al*. 1997). To determine whether the *in vivo* subcellular localization of the 81 aa exon 1 fragment of pathogenic

human Htt (HttQ96-GFP) differs from that of the 588 aa pathogenic Htt fragment in our *Drosophila* model, HttQ96-GFP-expressing 3rd instar larvae were imaged using confocal microscopy. In both neuronal and non-neuronal cell types, HttQ96-GFP formed distinct cytoplasmic aggregates similar in appearance and localization to those formed by the 588 aa mRFP-HttQ138 protein. GFP-labeled aggregates are found in the cytoplasm of salivary gland cells (Figure 5B) and CNS (Figure 5D) and PNS (Figure 5G) neurons, while no aggregates are observed with expression of a UAS-GFP construct alone (Figure 5A, C, F). As observed with the 588 aa fragment, the exon 1 fragment also forms aggregates in axons (Figure 5E) and localizes at nerve terminals. The localization of both 588 aa and 81 aa pathogenic Htt fragments indicates that the neurodegenerative effects induced by these toxic Htt forms are independent of Htt nuclear accumulation in *Drosophila*. In addition, targeting sequences in exon 1 of Htt are sufficient to localize the protein to neurites in our model.

Kinetics of HttQ138 aggregate formation: To examine how Htt aggregates form, we visualized mRFP-HttQ138 dynamics in live larvae. We expressed mRFP-HttQ138 using *CCAP*-GAL4 that expresses in a single neuron per hemisegment (PARK *et al*. 2003; VOMEL and WEGENER 2007). This driver allows single cell resolution for assaying how soluble HttQ138 interacts with larger aggregates. Time-lapse confocal imaging in 3rd instar larval motor neurons expressing mRFP-HttQ138 demonstrate that large aggregates are immobile over a two hour imaging session. FRAP analysis reveals that HttQ138-positive photobleached aggregates continually add new HttQ138 particles, with a 40% recovery of original fluorescence within 50 minutes (Figure 6A-C, Supplemental Video 1). Two general types of recovery were observed. Larger HttQ138 aggregates tend to recover more quickly by trapping Htt particles (right-most

aggregate in Supplemental Video 1). A second class of aggregates recover more slowly and display a gradual and uniform increase in brightness (left three aggregates in Supplemental Video 1). To determine if the rapid FRAP in axons was due to increased flux of HttQ138 mediated by delivery of new particles by fast axonal transport (FAT), we compared FRAP rates of aggregates in axons to that in neuronal cell bodies aggregates where HttQ138 movement is dictated largely by diffusion. We did not observe a significant difference in aggregation kinetics in these two compartments, indicating that axonal aggregation kinetics are not strictly dependent on FAT (Figure 6B).

We next examined the kinetics of *de novo* HttQ138 aggregate formation in our model *in vivo*. During our time-lapse imaging sessions in 3rd instar larvae, we did not observe new aggregates forming. We attempted to visualize aggregate formation in younger animals, but numerous aggregates were already present at the 1st instar larval stage. It appeared that aggregates formed early in development grew, but that new aggregates rarely formed in the presence of preexisting ones. To bypass this problem, we used the temperature-sensitive GAL80 repressor to restrict expression of mRFP-HttQ138 through the 2nd instar stage. Expression of mRFP-HttQ138 with the *CCAP*-GAL4 driver was repressed by GAL80^{ts} at 18°C until the larvae reached 3rd instar. We then turned on HttQ138 expression by shifting animals to the GAL80^{ts} restrictive temperate of 30°C. Two hours after induction of expression, a low level of diffuse mRFP-HttQ138 was observed in the salivary gland. By four hours, small Htt aggregates were observed forming in the salivary gland (Figure 7). After eight hours of expression, diffuse mRFP-HttQ138 was seen in neuronal cell bodies in the ventral nerve cord, as well as in the proximal regions of axons. By 12 hours, aggregates were seen forming in axons and cell bodies, while salivary gland aggregates increased in size. During the window from 12-24 hours after

induction, aggregates became larger and more numerous (Figure 7). Beyond 12 hours post-induction, HttQ138 aggregates began growing in size rather than number. The increase in aggregated mRFP-HttQ138 was accompanied by a decrease in the soluble fraction of the protein. We also examined the effectiveness of reducing aggregation by turning off expression of the mRFP-HttQ138 transgene after aggregates had formed, assaying if cells had the ability to remove aggregates without new HttQ138 expression. After a 24-hour pulse of mRFP-HttQ138 expression followed by 72 hours of recovery, we observed a reduction in the size and number of aggregates present (Figure 7). We conclude that new aggregates can form in neurons within 12 hours, while pre-existing aggregates rapidly accumulate new HttQ138 protein within minutes. In addition, in the absence of new Htt protein synthesis, neurons are capable of reducing preexisting Htt aggregate size over time.

mRFP-HttQ138 induced lethality can be rescued by heterozygous disruption of single loci: To further define the role of aggregation in HD pathology, we performed forward genetic screens for suppressors of HttQ138-induced lethality or suppressors of HttQ138 aggregation. For the first screen to identify lethality suppressors, we employed a dominant suppressor strategy with the *Drosophila* autosomal deficiency (Df) set to identify chromosomal regions containing loci that could dominantly rescue mRFP-HttQ138-induced lethality. We reasoned that loci identified in a haplo-insufficiency screen might represent attractive targets for ameliorating HD pathology, as a 50% decrease in protein activity might require only partial reduction of the protein's function through pharmacological approaches. We obtained the Df kit for chromosomes II and III from the Bloomington Stock Center, which contains 160 Df lines that cover ~80% of the *Drosophila* genome. We crossed Df/Balancer males to females carrying the *elav*-GAL4 driver homozygous

on the X chromosome (C155) and a marked Balancer, with *CyO* for the 2nd chromosome and *Sb* or *Hu* for the 3rd chromosome. F1 C155/y; Df/Bal offspring were then mated to homozygous mRFP-HttQ138 high expression females. Under normal conditions, expression of mRFP-HttQ138 driven by C155 caused pharate adult lethality. We screened for Dfs that rescued this lethality, comparing the number of adult females expressing mRFP-HttQ138 to males not expressing the HttQ138 transgene. Deficiencies that dominantly increased the ratio of mRFP-HttQ138 expressing females by 10-fold (Female/Male ratio = 0.1) were identified as hits. We identified 11 large Dfs, each removing ~100 genes, that suppressed HttQ138-induced lethality, indicating the presence of multiple potential targets that can modify HttQ138 toxicity in a dominant manner (Figure 8A, Supplemental Table 1). Ten out of 11 deletions gave a partial rescue of viability, increasing the number of escapers to ~20-30% of that expected for a full rescue. The viable animals displayed motor defects, as they were unable to climb the walls of the vials or mate, and most died within several days of eclosion, indicating partial rescue. One of the 11 large deletions, *Df(3L)vin7* showed a near complete rescue of viability at eclosion. C155; *Df(3L)vin7*/mRFP-HttQ138 animals showed less severe motor defects than other rescuing Dfs, but were unable to climb the vial walls and lived ~10 days post-eclosion.

Reduction of HttQ138 expression and aggregation increases viability in mRFP-HttQ138 expressing *Drosophila:* In addition to the viability screen, we conducted a screen for suppressors of aggregation. The same mating scheme was used in both screens. However the aggregation screen used the lower expression adult-viable mRFP-HttQ138B insert, instead of the pharate lethal high expression mRFP-HttQ138 line. We reasoned the lower expression line would represent a more sensitized system to identify potentially weak aggregation suppressors

that might not be found in strong expression strains. Live wandering 3rd instar larvae expressing mRFP-HttQ138 and hetererozygous for each Df were screened under a fluorescent microscope for changes in aggregation. We focused on Htt aggregation within the salivary gland, as these large cells were easily visualized in live animals. We screened for changes in size, density or brightness of peri-nuclear mRFP-Htt salivary gland aggregates. Four large deletions (*Df(2R)59AD, Df(2R)AA21, Df(2R)cn9* and *Df(3L)vin7*) caused a reduction in aggregate density in the salivary gland (Figure 8B-F). Interestingly, each of these aggregation suppressors was independently identified in the viability screen. Thus, reducing aggregation in our screen was always associated with increased viability. We did not identify any hits that reduced aggregation without increasing viability, suggesting that aggregates may represent a toxic species in this model. While *Df(2R)59AD* reduced the density and size of salivary gland aggregates, *Df(2R)cn9*, *Df(3L)vin7* and *Df(2R)AA21* were most effective in reducing aggregation, with the mRFP-Htt Q138 pattern appearing as diffuse as the nonpathogenic mRFP-HttQ15. We attempted finer mapping for each larger Df to define the smallest relevant genetic interval. We were able to map the *Df(2R)59AD* interval to a region uncovered by *Df(2R)59AB*, which deletes ~ 20 genes. The larger *Df(2R)cn9* was subdivided to a critical region uncovered by *Df(2R)sple-J1*, which removes ~39 genes.

To determine whether suppression of aggregation was associated with a change in mRFP-HttQ138 expression, we quantified Western blots of flies expressing mRFP-HttQ138 with C155 in the Df background (Figure 9A, B). As a control for UAS-GAL4 transgene regulation, we also quantified expression of UAS-CD8-GFP in the Df backgrounds (Figure 9C). All four deletions that reduced aggregation resulted in reduced mRFP-HttQ138 and CD8-GFP protein expression. However, two single gene suppressors (*lab*[14], PBc02324 – see below) had no effect on salivary

gland aggregation or transgenic protein expression by Western analysis. To further characterize the suppressors, we measured HttQ138 mRNA levels using semi-quantitative RT-PCR. Despite showing distinct effects on protein level, all Dfs decreased HttQ138 mRNA levels. These results are consistent with the observation that Htt aggregation is strongly influenced by expression levels of the protein, and that toxicity in our model correlates with HttQ138 expression level (Figure 1C).

We next determined whether the reduction in salivary gland HttQ138 aggregates and suppression of lethality by these Dfs resulted in alteration in the subcellular distribution or density of Htt aggregates in peripheral nerves. Htt aggregates in axons have been suggested to cause axonal transport defects and contribute to HD pathogenesis (GUNAWARDENA *et al.* 2003; LEE *et al.* 2004; LI *et al.* 1999; LI *et al.* 2001). We found a significant ($p<0.05$) decrease in the number of mRFP-HttQ138 aggregates >1μm diameter in axons in the *Df(3L)vin7* background, but no change in the other Dfs (Figure 10). Interestingly, *Df(3L)vin7* had the strongest effect on suppressing lethality (Supplemental Figure 1) and improving motor performance in HttQ138 expressing animals. We also analyzed Syt 1 distribution along axons, which we have previously observed to co-aggregate with Htt in axonal aggregations (LEE *et al.* 2004), while remaining diffuse in axons from controls or HttQ15-expressing animals. Abnormal aggregation of Syt 1 was still observed in the rescued animals (Figure 10A-G), indicating that although the Dfs reduced aggregation in salivary glands and suppressed lethality, they did not prevent axonal aggregation of HttQ138. The identification of dosage-sensitive suppressors of mutant Htt toxicity that reduce lethality without disrupting aggregation suggests that pathways downstream of aggregate formation can be targeted for neuroprotection in HD. The differences in HttQ138 mRNA levels versus HttQ138 aggregates also suggest that subtle changes in transcript level can

have a dramatic effect on the concentration reached within a cell that is required to trigger aggregation.

Mapping of suppressors of HttQ138-induced lethality: To begin identifying loci that underlie suppression of HttQ138-induced phenotypes, we attempted finer mapping of hits from the viability and aggregation screen by testing smaller and overlapping Dfs within these regions using stocks available from the Bloomington stock center. In many cases, coverage across the original Df region was not sufficient to map suppression to individual loci. It is also possible that the ability of some Dfs to suppress toxicity may have resulted from additive effects of haplo-insufficiency for several genes within the deleted region. However, we were able to successfully refine three of the original 11 large deletions to two individual loci. The large Df suppressors *Df(3L)st-f13* and *Df(3L)brm11* overlapped a 43-gene region from 72C1-72D5. *Df(3L)ED220* further refined the area to 72C1-72D4, a 20-gene interval with mutant stocks available for 12 predicted loci (Supplemental Figure 1). We tested the 12 lines and observed that stock 10887 rescued HttQ138 expressing animals at greater than the 10% expected ratio. Line 10887 (PBc02324) is a *piggyBac* transposable element insertion into the 5' region between two genes, CG5830 and *mRpS31*. RT-PCR of line 10887 revealed that CG5830 is downregulated 2-fold, while *mRpS31* is not significantly affected by the insertion (Supplemental Figure 2). CG5830 is 60% identical to mammalian CTD phosphatases, which function in silencing neuronal gene expression. The repressor element 1/neuron-restrictive silencer element (REST) transcription repressor family is essential for neuronal gene silencing and has been linked to HD (RIGAMONTI *et al.* 2009).

The remaining interval we were able to refine to a single mutation was *Df(3R)Tpl10*, which deletes the 83C1-84B2 region and uncovers 173 genes. Screening other Dfs in this region revealed that *Df(3R)MAP117* and *Df(3R)MAP2* significantly rescued viability of HttQ138 expressing animals. These Dfs overlap the 84A1 to 84A5 interval, which contains 47 genes with 18 stocks available that disrupt loci within. We tested these strains and found that stock 2092 rescued mRFP-HttQ138 induced lethality, increasing the expected adult viability ratio to 24% versus 0% in strains expressing HttQ138 alone. Stock 2092 is an x-ray induced amorphic mutant (lab^{14}) of the *labial* gene. *Labial* is one of eight homeobox genes in the Antennapedia cluster that play critical developmental roles in anterior-posterior body axis specification (BRODY 1999). To determine if other members of the Antennapedia HOX complex could also suppress HD pathology in our model, we tested mutations in additional members of the Antennapedia cluster for their ability to rescue HttQ138-induced lethality. Haplo-insufficiency for mutations in *Sex combs reduced* (Scr^{CP1} - 22% viability ratio; Scr^{6} - 24% viability ratio), *proboscopedia* (pr^{1} - 22% viability ratio), *Deformed* (Dfd^{6} - 15% viability ratio) and *Ultrabithorax* (Ubx^{51} - 12% viability ratio) also resulted in a significant rescue of HttQ138-induced lethality.

Both aggregated and soluble HttQ138 are likely to represent toxic species: By comparing the relative contributions of decreased aggregation and decreased soluble HttQ138 measured experimentally to increased lifespan, we observed a general trend whereby decreasing Htt expression causes a decrease in aggregation and increase in viability (Figure 11). However, two suppressors uncovered in the screen displayed increased viability without a significant change in aggregation in peripheral motor axons (*Df(2R)59AB* and *Df(2R)sple-j1*). mRFP-HttQ138 expression in these backgrounds is decreased by Western analysis and RT-PCR, but there is no

change in the number of axonal aggregates (Figure 8C, E). Additionally, *Pbc020324* and *lab*^{14} show increased lifespan without a significant change in aggregation in any cell type. These suppressor backgrounds indicate some increase in viability can be achieved independent of decreasing aggregated HttQ138. In these lines, the increase in lifespan is correlated with a decrease in soluble HttQ138, arguing that this form of HttQ138 may also contribute to toxicity.

Discussion

Many neurodegenerative diseases associated with protein misfolding have been modeled in *Drosophila*, including Parkinson's disease (FEANY and BENDER 2000), Alzheimer's disease (WITTMANN *et al*. 2001), spinocerebellar ataxia type 1 (FERNANDEZ-FUNEZ *et al*. 2000) and type 3 (WARRICK *et al*. 1999) and Huntington's disease (GUNAWARDENA *et al*. 2003; JACKSON *et al*. 1998; LEE *et al*. 2004; STEFFAN *et al*. 2001). These models replicate many neuropathological features characteristic of the diseases, such as late onset, progressive neurodegeneration, and formation of inclusions containing the mutant protein. Here we describe the generation of a new *Drosophila* HD model in which expression of a 588 aa N-terminal fragment of human Htt containing a 138 polyQ tract results in pharate adult lethality. By engineering a fluorescent tag on the mutant Htt fragment, we were able to visualize the location, trafficking and aggregation of Htt in both neuronal and non-neuronal cells in live *Drosophila*. As such, we were able to screen independently for suppressors of Htt aggregation by following HttQ138-mRFP localization in live animals. The screens resulted in the identification of seven large Dfs uncovering genomic regions that are capable of suppressing Htt-induced lethality without altering HttQ138 aggregate formation, and four additional Dfs that suppressed both Htt-induced lethality and HttQ138 aggregation. Our findings indicate the presence of gene products downstream, or independent, of

aggregation that can dominantly reduce HD toxicity. Our results also indicate that expression levels of mutant Htt are critical for disease pathology, as all Dfs we identified that reduced Htt expression levels by ~50% increased viability. As such, targeted approaches that reduce mutant Htt expression by relatively modest amounts may have profound effects on toxicity in HD patients.

The ability to follow Htt dynamics in live animals using our fluorescently-tagged HttQ15 and HttQ138 trangenes revealed several important aspects of our *Drosophila* HD model. We find that both pathogenic and nonpathogenic versions of Htt are localized to the cytoplasm of all cell types examined. In humans, cleavage of Htt is thought to be important in generation of toxic Htt fragments (QIN and GU 2004), with several studies indicating that small cleaved N-terminal fragments enter the nucleus to form intranuclear inclusions that contribute to pathogenesis (DIFIGLIA *et al*. 1997; SIERADZAN *et al*. 1999). Although evidence suggests that intranuclear aggregates can contribute to HD pathology (BECHER *et al*. 1998; DAVIES *et al*. 1997), several studies indicate that pathogenic Htt aggregates in the cytoplasm and neurites play a causative role (LI *et al*. 1999; SAPP *et al*. 1999). As such, where toxic Htt fragments responsible for HD pathology reside in neurons remains to be conclusively identified. Using Htt fragments that were tagged at the N-terminus with GFP and at the C-terminus with mRFP, we demonstrate that cleavage of Htt is not apparent in *Drosophila*. In addition, expression of a smaller Htt Exon 1 fragment still localizes to the cytoplasm. It is possible that addition of a GFP moiety alters Htt localization, although we observed the same pattern with an HA-tagged Htt transgenic protein as well (LEE *et al*. 2004). Thus, pathology in this HD model occurs secondary to cytoplasmic polyQ Htt localization.

To characterize the kinetics of Htt aggregation, we used live imaging of fluorescently tagged mRFP-HttQ138. Several studies indicate mutant Htt can disrupt FAT (GUNAWARDENA *et al*. 2003; LEE *et al*. 2004; SZEBENYI *et al*. 2003), but the mechanism by which defects occur is unclear. Since Htt is selectively toxic to neurons, an attractive model is that disrupted FAT may confer toxicity due to transport defects. Our FRAP data suggests that large immobile aggregates acquire new HttQ138 puncta. We determined the rate of FRAP recovery within aggregates was the same in both axons and the cell body, suggesting that aggregation kinetics are not solely dependent on the higher local concentrations of Htt induced by FAT. We took advantage of the Gal80^{ts} repressor to view early events in aggregate formation and visualize the aggregation progression. We observed that soluble HttQ138 forms aggregates that grow in size over a 12-hour window, decreasing the amount of soluble Htt present in the cell. Incorporation of HttQ138 into pre-existing aggregrates was much faster, suggesting once aggregates are formed, they represent an active sink for accumulating new Htt protein on a minute timescale.

A key question in the HD field is whether Htt aggregates are toxic, neuroprotective or simply byproducts of the disease process. This issue is of critical importance for therapeutic considerations, as many current efforts are aimed at reducing Htt aggregation, assuming that this will decrease toxicity. Our previous observations that Htt aggregates accumulate in axons and impede axonal transport (LEE *et al*. 2004) suggested a model in which axonally localized aggregates can disrupt neuronal function. Whether aggregates in other cellular compartments cause toxicity is still an open question. The ability of drugs like Congo Red (HEISER *et al*. 2000; SANCHEZ *et al*. 2003), minocycline (CHEN *et al*. 2000; SMITH *et al*. 2003), and the transglutaminase inhibitor cystamine (DEDEOGLU *et al*. 2002) to block Htt aggregation and reduce behavioral phenotypes in R6/2 Htt polyQ mice is suggestive of aggregate toxicity as well.

Molecular (CUMMINGS *et al*. 2001; FERNANDEZ-FUNEZ *et al*. 2000; JANA *et al*. 2000; VACHER *et al*. 2005; WARRICK *et al*. 1999) and chemical (YOSHIDA *et al*. 2002) chaperones that reduce aggregate formation have been shown to reduce cytotoxicity in several polyQ disease models. Likewise, intracellular antibodies (COLBY *et al*. 2004; KHOSHNAN *et al*. 2002; LECERF *et al*. 2001; WOLFGANG *et al*. 2005) that bind mutant Htt epitopes and suppress aggregate formation provide some neuroprotection in animal models. Our genetic screens support a model where aggregate formation and soluble Htt (monomers or oligomers) may both contribute to toxicity, as every Df which reduced aggregation or soluble Htt levels showed an increase in viability. The observation that we did not identify any haplo-insufficient loci capable of reducing aggregation without altering Htt expression levels suggests that aggregation inhibition alone may require more potent pharmacological effects than can be achieved with only a 50% reduction in activity of a single protein. In contrast, the finding that *Df(2R)spleJ1* and *Df(2R)59AB* increase viability without changes in aggregation suggests that HttQ138 toxicity can be reduced without altering Htt aggregation.

Although neuronal toxicity associated with Htt polyQ expansion has been the emphasis of most HD studies, the Htt protein is expressed in many nonneuronal tissues, including testes, liver, heart, lungs, and pancreatic islets (CATTANEO *et al*. 2005; FERRANTE *et al*. 1997). HD patients have been shown to have a higher risk of diabetes (LALIC *et al*. 2008), and mouse HD models show pancreatic pathology (MARTIN *et al*. 2008), indicating that Htt polyQ expansion may also cause defects in non-neuronal cells. We found that HttQ138 expression in *Drosophila* salivary glands results in defective glue secretion (Figure 3), suggesting that non-neuronal defects from HttQ138 expression exist in our model as well. The ease with which the Sgs3-GFP glue secretion assay can be performed opens up the possibility of additional screens for second-

site suppressors that alleviate salivary gland dysfunction in HttQ138 expressing animals. It is currently unclear whether salivary cell Htt aggregates induce pathology, or whether they are secondary to other defective secretion mechanisms. Htt is associated with numerous organelles, including the Golgi, ER, clathrin-coated vesicles, synaptic vesicles and endosomal vesicles (HOFFNER *et al*. 2002; KEGEL *et al*. 2002; VELIER *et al*. 1998). In addition, Htt interacts with numerous vesicle trafficking proteins, including dynamin, huntingtin-interacting protein 1 (HIP1), and huntingtin-associated protein1 (HAP1), which binds the p150glued subunit of dynactin (LI *et al*. 1998). Potential defects in vesicle trafficking or fusion may thus account for the defects observed in glue secretion.

The results from our haplo-insufficiency screen provide several clues regarding the role of soluble and aggregated forms of Htt and their contribution to toxicity, but no clear information about cellular pathways disrupted by HD. We mapped the suppression mediated by three large Dfs down to two single genes. One of our hits was a *piggyBac* insertion in strain PBc020324 in the small 5' interval between CG5830 and *mRpS3,* which reduces CG5830 expression. CG5830 encodes a phosphatase with sequence homology to small CTD phosphatases that function in silencing neuronal gene expression (YEO *et al*. 2005). Disruption of neurotrophic factor expression, especially BDNF through aberrant function of its transcriptional repressor REST/NRSF, has been implicated in HD mouse models and in HD patients cortex (BUCKLEY *et al*. 2010; ZUCCATO *et al*. 2007; ZUCCATO *et al*. 2001). It will be important to test whether previously identified *Drosophila* neurotrophic proteins (ZHU *et al*. 2008) are disregulated in mRFP-HttQ138 expressing animals, and whether haplo-insufficiency of CG5830 reduces this effect. Although Pbc020324 is likely rescuing toxicity in part by reducing Htt transgene expression, we did not observe any decrease in HttQ138 aggregation or protein levels by

Western analysis. This discrepancy between reduced transcription and Htt protein levels and aggregation suggests CG5830 may have other neuroprotective effects as well.

The other single gene we mapped, *Labial* is a member of the ANTP complex, and has been linked to neural stem cell survival during postembryonic neurogenesis in *Drosophila* (BELLO *et al*. 2007). Mutant Htt has been implicated in transcriptional dysregulation of a broad range of genes, reducing levels of highly pleiotropic proteins like RNA polymerase II (LUTHI-CARTER *et al*. 2002), and facilitating expression in mice of polycomb repressive complex 2, which specifically regulates HOX gene expression (SEONG *et al*.). Htt has also been linked to HOX gene regulation through the polyQ and poly-Proline regions shared between Htt and several transcriptional regulators, including *Sex combs reduced* (GERBER *et al*. 1994). Similar to Pbc020324, this mutation decreases Htt transgene transcription, but has no effect on aggregation. The decreased Htt transcription in the *hox* mutants likely contributes to the suppressive effects of these strains. However, an additional effect suggested by microarray analysis of Htt-polyQ expressing brains in *Drosophila* (Lee and Littleton, unpublished data) is that ANTP genes are upregulated in HD and contribute to neuropathology. Several Hox genes, including *labial*, *proboscipedia,* and *Sex combs reduced* were increased in Htt-polyQ brains, suggesting that haplo-insufficiency for these loci might function to reduce Htt expression to a less toxic level. Further studies will be needed to dissect this link between the homeotic genes and HD pathology.

Examining the pattern by which suppressor mutations interact with HttQ138 provides insight into the role of aggregates in toxicity. The weakest suppressors had no alteration in aggregation or HttQ138 expression, suggesting some minor rescue is possible without disrupting aggregation. A larger increase in viability occurs with decreased expression of HttQ138, but little to no change in aggregated Htt, suggesting that soluble HttQ138 is a toxic species in these cases.

The final group of suppressors increased viability even more, while decreasing both soluble and aggregated Htt. In summary, we have generated a new HD model in *Drosophila* that allows for *in vivo* analysis of pathogenic Htt localization, aggregation and dynamics. Using this model, we identified several genetic suppressors that can reduce HttQ138-mediated toxicity. The most robust suppressors reduced both soluble and aggregated Htt levels, suggesting that toxicity is likely to be associated with both forms of the mutant protein.

Acknowledgments

We thank David Housman for kindly providing the HttQ96-GFP construct, Katie Lynch for help with subcloning the HttQ96-GFP construct, Albert Su, Grace Lin and Rupali Avasare for S2 cell experiments, Andrew Andres for providing the Sgs3-GFP expressing *Drosophila* and Ray Truant for HttQ15 and HttQ138 cDNAs.

References:

ARRASATE, M., S. MITRA, E. S. SCHWEITZER, M. R. SEGAL and S. FINKBEINER, 2004 Inclusion body formation reduces levels of mutant huntingtin and the risk of neuronal death. Nature **431:** 805-810.

BECHER, M. W., J. A. KOTZUK, A. H. SHARP, S. W. DAVIES, G. P. BATES *et al.*, 1998 Intranuclear neuronal inclusions in Huntington's disease and dentatorubral and pallidoluysian atrophy: correlation between the density of inclusions and IT15 CAG triplet repeat length. Neurobiology of Disease **4:** 387-397.

BELLO, B., N. HOLBRO and H. REICHERT, 2007 Polycomb group genes are required for neural stem cell survival in postembryonic neurogenesis of Drosophila. Development **134:** 1091-1099.

BIYASHEVA, A., T. V. DO, Y. LU, M. VASKOVA and A. J. ANDRES, 2001 Glue secretion in the Drosophila salivary gland: a model for steroid-regulated exocytosis. Developmental Biology **231:** 234-251.

BRODY, T., 1999 The Interactive Fly: gene networks, development and the Internet. Trends in Genetics : TIG **15:** 333-334.

BUCKLEY, N. J., R. JOHNSON, C. ZUCCATO, A. BITHELL and E. CATTANEO, 2010 The role of REST in transcriptional and epigenetic dysregulation in Huntington's disease. Neurobiol Dis **39:** 28-39.

CAMPBELL, R. E., O. TOUR, A. E. PALMER, P. A. STEINBACH, G. S. BAIRD *et al.*, 2002 A monomeric red fluorescent protein. Proceedings of the National Academy of Sciences of the United States of America **99:** 7877-7882.

CARMICHAEL, J., J. CHATELLIER, A. WOOLFSON, C. MILSTEIN, A. R. FERSHT *et al.*, 2000 Bacterial and yeast chaperones reduce both aggregate formation and cell death in mammalian cell models of Huntington's disease. Proceedings of the National Academy of Sciences of the United States of America **97:** 9701-9705.

CATTANEO, E., C. ZUCCATO and M. TARTARI, 2005 Normal huntingtin function: an alternative approach to Huntington's disease. Nature Reviews Neuroscience **6:** 919-930.

CHAI, Y., J. SHAO, V. M. MILLER, A. WILLIAMS and H. L. PAULSON, 2002 Live-cell imaging reveals divergent intracellular dynamics of polyglutamine disease proteins and supports a sequestration model of pathogenesis. Proceedings of the National Academy of Sciences of the United States of America **99:** 9310-9315.

CHEN, M., V. O. ONA, M. LI, R. J. FERRANTE, K. B. FINK *et al.*, 2000 Minocycline inhibits caspase-1 and caspase-3 expression and delays mortality in a transgenic mouse model of Huntington disease. Nature Medicine **6:** 797-801.

CHOPRA, V., J. H. FOX, G. LIEBERMAN, K. DORSEY, W. MATSON *et al.*, 2007 A small-molecule therapeutic lead for Huntington's disease: preclinical pharmacology and efficacy of C2-8 in the R6/2 transgenic mouse. Proceedings of the National Academy of Sciences of the United States of America **104:** 16685-16689.

COLBY, D. W., Y. CHU, J. P. CASSADY, M. DUENNWALD, H. ZAZULAK *et al.*, 2004 Potent inhibition of huntingtin aggregation and cytotoxicity by a disulfide bond-free single-domain intracellular antibody. Proceedings of the National Academy of Sciences of the United States of America **101:** 17616-17621.

CUMMINGS, C. J., Y. SUN, P. OPAL, B. ANTALFFY, R. MESTRIL *et al.*, 2001 Over-expression of inducible HSP70 chaperone suppresses neuropathology and improves motor function in SCA1 mice. Human Molecular Genetics **10:** 1511-1518.

DAVIES, S. W., M. TURMAINE, B. A. COZENS, M. DIFIGLIA, A. H. SHARP *et al.*, 1997 Formation of neuronal intranuclear inclusions underlies the neurological dysfunction in mice transgenic for the HD mutation. Cell **90:** 537-548.

DEDEOGLU, A., J. K. KUBILUS, T. M. JEITNER, S. A. MATSON, M. BOGDANOV *et al.*, 2002 Therapeutic effects of cystamine in a murine model of Huntington's disease. The Journal of Neuroscience **22:** 8942-8950.

DIFIGLIA, M., E. SAPP, K. O. CHASE, S. W. DAVIES, G. P. BATES *et al.*, 1997 Aggregation of huntingtin in neuronal intranuclear inclusions and dystrophic neurites in brain. Science **277:** 1990-1993.

FEANY, M. B., and W. W. BENDER, 2000 A Drosophila model of Parkinson's disease. Nature **404:** 394-398.

FERNANDEZ-FUNEZ, P., M. L. NINO-ROSALES, B. DE GOUYON, W. C. SHE, J. M. LUCHAK *et al.*, 2000 Identification of genes that modify ataxin-1-induced neurodegeneration. Nature **408:** 101-106.

FERRANTE, R. J., C. A. GUTEKUNST, F. PERSICHETTI, S. M. MCNEIL, N. W. KOWALL *et al.*, 1997 Heterogeneous topographic and cellular distribution of huntingtin expression in the normal human neostriatum. The Journal of Neuroscience **17:** 3052-3063.

FUGER, P., L. B. BEHRENDS, S. MERTEL, S. J. SIGRIST and T. M. RASSE, 2007 Live imaging of synapse development and measuring protein dynamics using two-color fluorescence recovery after photo-bleaching at Drosophila synapses. Nature Protocols **2:** 3285-3298.

GAFNI, J., E. HERMEL, J. E. YOUNG, C. L. WELLINGTON, M. R. HAYDEN *et al.*, 2004 Inhibition of calpain cleavage of huntingtin reduces toxicity: accumulation of calpain/caspase fragments in the nucleus. The Journal of biological chemistry **279:** 20211-20220.

GERBER, H. P., K. SEIPEL, O. GEORGIEV, M. HOFFERER, M. HUG *et al.*, 1994 Transcriptional activation modulated by homopolymeric glutamine and proline stretches. Science **263:** 808-811.

GRAHAM, R. K., Y. DENG, E. J. SLOW, B. HAIGH, N. BISSADA *et al.*, 2006 Cleavage at the caspase-6 site is required for neuronal dysfunction and degeneration due to mutant huntingtin. Cell **125:** 1179-1191.

GUNAWARDENA, S., L. S. HER, R. G. BRUSCH, R. A. LAYMON, I. R. NIESMAN *et al.*, 2003 Disruption of axonal transport by loss of huntingtin or expression of pathogenic polyQ proteins in Drosophila. Neuron **40:** 25-40.

HARJES, P., and E. E. WANKER, 2003 The hunt for huntingtin function: interaction partners tell many different stories. Trends in Biochemical sciences **28:** 425-433.

HEISER, V., E. SCHERZINGER, A. BOEDDRICH, E. NORDHOFF, R. LURZ *et al.*, 2000 Inhibition of huntingtin fibrillogenesis by specific antibodies and small molecules: implications for Huntington's disease therapy. Proceedings of the National Academy of Sciences of the United States of America **97:** 6739-6744.

HODGSON, J. G., N. AGOPYAN, C. A. GUTEKUNST, B. R. LEAVITT, F. LEPIANE *et al.*, 1999 A YAC mouse model for Huntington's disease with full-length mutant huntingtin, cytoplasmic toxicity, and selective striatal neurodegeneration. Neuron **23:** 181-192.

HOFFNER, G., M. L. ISLAND and P. DJIAN, 2005 Purification of neuronal inclusions of patients with Huntington's disease reveals a broad range of N-terminal fragments of expanded huntingtin and insoluble polymers. Journal of Neurochemistry **95:** 125-136.

HOFFNER, G., P. KAHLEM and P. DJIAN, 2002 Perinuclear localization of huntingtin as a consequence of its binding to microtubules through an interaction with beta-tubulin: relevance to Huntington's disease. Journal of Cell Science **115:** 941-948.

JACKSON, G. R., I. SALECKER, X. DONG, X. YAO, N. ARNHEIM *et al.*, 1998 Polyglutamine-expanded human huntingtin transgenes induce degeneration of Drosophila photoreceptor neurons. Neuron **21:** 633-642.

JANA, N. R., M. TANAKA, G. WANG and N. NUKINA, 2000 Polyglutamine length-dependent interaction of Hsp40 and Hsp70 family chaperones with truncated N-terminal huntingtin: their role in suppression of aggregation and cellular toxicity. Human Molecular Genetics **9:** 2009-2018.

KEGEL, K. B., A. R. MELONI, Y. YI, Y. J. KIM, E. DOYLE *et al.*, 2002 Huntingtin is present in the nucleus, interacts with the transcriptional corepressor C-terminal binding protein, and represses transcription. The Journal of Biological Chemistry **277:** 7466-7476.

KHOSHNAN, A., J. KO and P. H. PATTERSON, 2002 Effects of intracellular expression of anti-huntingtin antibodies of various specificities on mutant huntingtin aggregation and toxicity. Proceedings of the National Academy of Sciences of the United States of America **99:** 1002-1007.

KIM, Y. J., Y. YI, E. SAPP, Y. WANG, B. CUIFFO *et al.*, 2001 Caspase 3-cleaved N-terminal fragments of wild-type and mutant huntingtin are present in normal and Huntington's disease brains, associate with membranes, and undergo calpain-dependent proteolysis. Proceedings of the National Academy of Sciences of the United States of America **98:** 12784-12789.

KIMURA, Y., W. C. LEE and J. T. LITTLETON, 2007 Therapeutic prospects for the prevention of neurodegeneration in Huntington's disease and the polyglutamine repeat disorders. Mini Reviews in Medicinal Chemistry **7:** 99-106.

KROBITSCH, S., and S. LINDQUIST, 2000 Aggregation of huntingtin in yeast varies with the length of the polyglutamine expansion and the expression of chaperone proteins. Proceedings of the National Academy of Sciences of the United States of America **97:** 1589-1594.

KUEMMERLE, S., C. A. GUTEKUNST, A. M. KLEIN, X. J. LI, S. H. LI *et al.*, 1999 Huntington aggregates may not predict neuronal death in Huntington's disease. Annals of Neurology **46:** 842-849.

LAJOIE, P., and E. L. SNAPP, 2010 Formation and toxicity of soluble polyglutamine oligomers in living cells. PloS One **5:** e15245.

LALIC, N. M., J. MARIC, M. SVETEL, A. JOTIC, E. STEFANOVA *et al.*, 2008 Glucose homeostasis in Huntington disease: abnormalities in insulin sensitivity and early-phase insulin secretion. Archives of Neurology **65:** 476-480.

LAM, W., W. M. CHAN, T. W. LO, A. K. WONG, C. C. WU *et al.*, 2008 Human receptor for activated protein kinase C1 associates with polyglutamine aggregates and modulates polyglutamine toxicity. Biochemical and Biophysical Research Communications **377:** 714-719.

LECERF, J. M., T. L. SHIRLEY, Q. ZHU, A. KAZANTSEV, P. AMERSDORFER *et al.*, 2001 Human single-chain Fv intrabodies counteract in situ huntingtin aggregation in cellular models of

Huntington's disease. Proceedings of the National Academy of Sciences of the United States of America **98:** 4764-4769.

LEE, W. C., M. YOSHIHARA and J. T. LITTLETON, 2004 Cytoplasmic aggregates trap polyglutamine-containing proteins and block axonal transport in a Drosophila model of Huntington's disease. Proceedings of the National Academy of Sciences of the United States of America **101:** 3224-3229.

LI, H., S. H. LI, A. L. CHENG, L. MANGIARINI, G. P. BATES *et al.*, 1999 Ultrastructural localization and progressive formation of neuropil aggregates in Huntington's disease transgenic mice. Human Molecular renetics **8:** 1227-1236.

LI, H., S. H. LI, Z. X. YU, P. SHELBOURNE and X. J. LI, 2001 Huntingtin aggregate-associated axonal degeneration is an early pathological event in Huntington's disease mice. The Journal of Neuroscience **21:** 8473-8481.

LI, S. H., C. A. GUTEKUNST, S. M. HERSCH and X. J. LI, 1998 Interaction of huntingtin-associated protein with dynactin P150Glued. The Journal of Neuroscience **18:** 1261-1269.

LUNKES, A., K. S. LINDENBERG, L. BEN-HAIEM, C. WEBER, D. DEVYS *et al.*, 2002 Proteases acting on mutant huntingtin generate cleaved products that differentially build up cytoplasmic and nuclear inclusions. Molecular Cell **10:** 259-269.

LUTHI-CARTER, R., S. A. HANSON, A. D. STRAND, D. A. BERGSTROM, W. CHUN *et al.*, 2002 Dysregulation of gene expression in the R6/2 model of polyglutamine disease: parallel changes in muscle and brain. Human Molecular Genetics **11:** 1911-1926.

MARTIN, B., E. GOLDEN, A. KESELMAN, M. STONE, M. P. MATTSON *et al.*, 2008 Therapeutic perspectives for the treatment of Huntington's disease: treating the whole body. Histology and Histopathology **23:** 237-250.

NAGAI, Y., T. INUI, H. A. POPIEL, N. FUJIKAKE, K. HASEGAWA *et al.*, 2007 A toxic monomeric conformer of the polyglutamine protein. Nature Structural & Molecular Biology **14:** 332-340.

ORR, H. T., and H. Y. ZOGHBI, 2007 Trinucleotide repeat disorders. Annual Review of Neuroscience **30:** 575-621.

PARK, J. H., A. J. SCHROEDER, C. HELFRICH-FORSTER, F. R. JACKSON and J. EWER, 2003 Targeted ablation of CCAP neuropeptide-containing neurons of Drosophila causes specific defects in execution and circadian timing of ecdysis behavior. Development **130:** 2645-2656.

PERSICHETTI, F., F. TRETTEL, C. C. HUANG, C. FRAEFEL, H. T. TIMMERS *et al.*, 1999 Mutant huntingtin forms in vivo complexes with distinct context-dependent conformations of the polyglutamine segment. Neurobiology of Disease **6:** 364-375.

PORTERA-CAILLIAU, C., J. C. HEDREEN, D. L. PRICE and V. E. KOLIATSOS, 1995 Evidence for apoptotic cell death in Huntington disease and excitotoxic animal models. The Journal of Neuroscience **15:** 3775-3787.

QIN, Z. H., and Z. L. GU, 2004 Huntingtin processing in pathogenesis of Huntington disease. Acta Pharmacologica Sinica **25:** 1243-1249.

RIECKHOF, G. E., M. YOSHIHARA, Z. GUAN and J. T. LITTLETON, 2003 Presynaptic N-type calcium channels regulate synaptic growth. The Journal of Biological Chemistry **278:** 41099-41108.

RIGAMONTI, D., C. MUTTI, C. ZUCCATO, E. CATTANEO and A. CONTINI, 2009 Turning REST/NRSF dysfunction in Huntington's disease into a pharmaceutical target. Current Pharmaceutical Design **15:** 3958-3967.

ROMERO, E., G. H. CHA, P. VERSTREKEN, C. V. LY, R. E. HUGHES *et al.*, 2008 Suppression of neurodegeneration and increased neurotransmission caused by expanded full-length huntingtin accumulating in the cytoplasm. Neuron **57:** 27-40.

SANCHEZ, I., C. MAHLKE and J. YUAN, 2003 Pivotal role of oligomerization in expanded polyglutamine neurodegenerative disorders. Nature **421:** 373-379.

SAPP, E., J. PENNEY, A. YOUNG, N. ARONIN, J. P. VONSATTEL *et al.*, 1999 Axonal transport of N-terminal huntingtin suggests early pathology of corticostriatal projections in Huntington disease. Journal of Neuropathology and Experimental Neurology **58:** 165-173.

SCHERZINGER, E., R. LURZ, M. TURMAINE, L. MANGIARINI, B. HOLLENBACH *et al.*, 1997 Huntingtin-encoded polyglutamine expansions form amyloid-like protein aggregates in vitro and in vivo. Cell **90:** 549-558.

SCHERZINGER, E., A. SITTLER, K. SCHWEIGER, V. HEISER, R. LURZ *et al.*, 1999 Self-assembly of polyglutamine-containing huntingtin fragments into amyloid-like fibrils: implications for Huntington's disease pathology. Proceedings of the National Academy of Sciences of the United States of America **96:** 4604-4609.

SEONG, I. S., J. M. WODA, J. J. SONG, A. LLORET, P. D. ABEYRATHNE *et al.*, 2010 Huntingtin facilitates polycomb repressive complex 2. Human Molecular Genetics **19:** 573-583.

SIERADZAN, K. A., A. O. MECHAN, L. JONES, E. E. WANKER, N. NUKINA *et al.*, 1999 Huntington's disease intranuclear inclusions contain truncated, ubiquitinated huntingtin protein. Experimental Neurology **156:** 92-99.

SINADINOS, C., T. BURBIDGE-KING, D. SOH, L. M. THOMPSON, J. L. MARSH *et al.*, 2009 Live axonal transport disruption by mutant huntingtin fragments in Drosophila motor neuron axons. Neurobiology of disease **34:** 389-395.

SLOW, E. J., R. K. GRAHAM, A. P. OSMAND, R. S. DEVON, G. LU *et al.*, 2005 Absence of behavioral abnormalities and neurodegeneration in vivo despite widespread neuronal huntingtin inclusions. Proc Natl Acad Sci U S A **102:** 11402-11407.

SMITH, D. L., B. WOODMAN, A. MAHAL, K. SATHASIVAM, S. GHAZI-NOORI *et al.*, 2003 Minocycline and doxycycline are not beneficial in a model of Huntington's disease. Annals of Neurology **54:** 186-196.

STEFFAN, J. S., L. BODAI, J. PALLOS, M. POELMAN, A. MCCAMPBELL *et al.*, 2001 Histone deacetylase inhibitors arrest polyglutamine-dependent neurodegeneration in Drosophila. Nature **413:** 739-743.

SZEBENYI, G., G. A. MORFINI, A. BABCOCK, M. GOULD, K. SELKOE *et al.*, 2003 Neuropathogenic forms of huntingtin and androgen receptor inhibit fast axonal transport. Neuron **40:** 41-52.

TAGAWA, K., M. HOSHINO, T. OKUDA, H. UEDA, H. HAYASHI *et al.*, 2004 Distinct aggregation and cell death patterns among different types of primary neurons induced by mutant huntingtin protein. Journal of Neurochemistry **89:** 974-987.

VACHER, C., L. GARCIA-OROZ and D. C. RUBINSZTEIN, 2005 Overexpression of yeast hsp104 reduces polyglutamine aggregation and prolongs survival of a transgenic mouse model of Huntington's disease. Human Molecular Genetics **14:** 3425-3433.

VELIER, J., M. KIM, C. SCHWARZ, T. W. KIM, E. SAPP *et al.*, 1998 Wild-type and mutant huntingtins function in vesicle trafficking in the secretory and endocytic pathways. Experimental Neurology **152:** 34-40.

VOMEL, M., and C. WEGENER, 2007 Neurotransmitter-induced changes in the intracellular calcium concentration suggest a differential central modulation of CCAP neuron subsets in Drosophila. Developmental Neurobiology **67:** 792-808.

VONSATTEL, J. P., R. H. MYERS, T. J. STEVENS, R. J. FERRANTE, E. D. BIRD *et al.*, 1985 Neuropathological classification of Huntington's disease. Journal of Neuropathology and Experimental Neurology **44:** 559-577.

WARRICK, J. M., H. Y. CHAN, G. L. GRAY-BOARD, Y. CHAI, H. L. PAULSON *et al.*, 1999 Suppression of polyglutamine-mediated neurodegeneration in Drosophila by the molecular chaperone HSP70. Nature Genetics **23:** 425-428.

WELLINGTON, C. L., L. M. ELLERBY, C. A. GUTEKUNST, D. ROGERS, S. WARBY *et al.*, 2002 Caspase cleavage of mutant huntingtin precedes neurodegeneration in Huntington's disease. The Journal of Neuroscience **22:** 7862-7872.

WITTMANN, C. W., M. F. WSZOLEK, J. M. SHULMAN, P. M. SALVATERRA, J. LEWIS *et al.*, 2001 Tauopathy in Drosophila: neurodegeneration without neurofibrillary tangles. Science **293:** 711-714.

WOLFGANG, W. J., T. W. MILLER, J. M. WEBSTER, J. S. HUSTON, L. M. THOMPSON *et al.*, 2005 Suppression of Huntington's disease pathology in Drosophila by human single-chain Fv antibodies. Proceedings of the National Academy of Sciences of the United States of America **102:** 11563-11568.

YEO, M., S. K. LEE, B. LEE, E. C. RUIZ, S. L. PFAFF *et al.*, 2005 Small CTD phosphatases function in silencing neuronal gene expression. Science **307:** 596-600.

YOSHIDA, H., T. YOSHIZAWA, F. SHIBASAKI, S. SHOJI and I. KANAZAWA, 2002 Chemical chaperones reduce aggregate formation and cell death caused by the truncated Machado-Joseph disease gene product with an expanded polyglutamine stretch. Neurobiology of Disease **10:** 88-99.

ZHU, B., J. A. PENNACK, P. MCQUILTON, M. G. FORERO, K. MIZUGUCHI *et al.*, 2008 Drosophila neurotrophins reveal a common mechanism for nervous system formation. PLoS biology **6:** e284.

ZUCCATO, C., A. CIAMMOLA, D. RIGAMONTI, B. R. LEAVITT, D. GOFFREDO *et al.*, 2001 Loss of huntingtin-mediated BDNF gene transcription in Huntington's disease. Science **293:** 493-498.

ZUCCATO, C., M. TARTARI, A. CROTTI, D. GOFFREDO, M. VALENZA *et al.*, 2003 Huntingtin interacts with REST/NRSF to modulate the transcription of NRSE-controlled neuronal genes. Nature Genetics **35:** 76-83.

Figure Legends

Figure 1. Generation of *Drosophila* transgenic models of HD. (A) The N-terminal fragments of human Htt used for transgenic construction are shown. PolyQ tracts and fluorescent tags (mRFP, eGFP) are indicated. The full-sized Htt protein is depicted for comparison. (B) Expression of Htt in control, mRFP-Htt, eGFP-Htt, and HttQ96-GFP strains with transgene expression driven by C155. Western blotting was performed with an antibody to the N-terminus of human Htt (mRFP-Htt and eGFP-Htt blot – left panel) or an antibody to GFP (HttQ96-GFP blot – right panel). (C) Reduced viability of transgenic strains expressing mutant Htt with a weaker *elav*-GAL4 driver. T_{50} is decreased by over 70% in strains expressing mRFP-HttQ138, 30% in strains expressing mRFP-HttQ138B (a lower expression strain), and 50% in strains expressing HttQ96-GFP, in comparison to control white flies crossed to the same driver.

Figure 2. Cytoplasmic aggregation of mRFP-HttQ138 in neuronal and non-neuronal tissues. (A) Htt localization in *Drosophila* S2 cells transiently transfected with mRFP-HttQ15 or mRFP-HttQ138. mRFP-HttQ15 is found diffusely throughout the cytoplasm, while mRFP-HttQ138 forms cytoplasmic aggregates. The scale bar is 2 μm for each panel. (B) Visualization of mRFP-HttQ15 (magenta) and GFP with a nuclear localization signal (nls) (green) in 3rd instar larvae with transgene expression driven by the C155. mRFP-HttQ15 is diffusely localized in the cytoplasm of CNS neurons in the ventral nerve cord. (C) Visualization of mRFP-HttQ138 (magenta) and GFP-nls (green) in CNS neurons of 3rd instar larvae with transgene expression driven by C155. Unlike mRFP-HttQ15, mRFP-HttQ138 forms cytoplasmic aggregates throughout the cell bodies of ventral nerve cord neurons. (D, E) Visualization of mRFP-Htt in

peripheral MD neurons. While mRFP-HttQ15 exhibits diffuse cytoplasmic localization, mRFP-HttQ138 is found in cytoplasmic aggregates throughout the cell body and neurites. (F-I) Expression of mRFP-Htt (magenta) and GFP-nls (green) driven by the *tubP*-GAL4 driver in the epidermis (F, G) and salivary gland (H, I). In all cases, mRFP-HttQ15 is diffuse throughout the cytoplasm, while mRFP-HttQ138 forms cytoplasmic aggregates.

Figure 3. Salivary gland glue secretion is defective in *Drosophila* expressing mRFP-HttQ138. (A) Pupa were removed from vials of CS (A), Htt-Q15 (B) or HttQ138 (C) animals expressing the Sgs3 GFP-tagged glue protein. Confocal images of Sgs3-GFP fluorescence are shown in the left panels and mRFP-Htt fluorescence in the right panel. (A) The Sgs3-GFP glue protein can be readily seen in the left panel lining the exterior surface of the pupal case (arrows) following secretion from salivary glands. CS animals do not express Htt-mRFP, with only minor autofluorescence visible in the red channel (right panel). (B) Glue secretion (arrows) is not disrupted in pupae that express mRFP-HttQ15, which localizes diffusely in the salivary gland (arrowhead). (C) Glue secretion is decreased in pupae expressing mRFP-HttQ138, with the Sgs3-GFP protein largely retained in salivary glands (arrows). Aggregation of mRFP-HttQ138 in the pupal salivary glands is noted by the arrowhead in the right panel. (D) Sgs3-GFP is abundant in CS 3rd instar larval salivary glands before pupation, and depleted from salivary glands following secretion during pupation (E). (F) Sgs3-GFP is retained in pupal salivary glands of mRFP-HttQ138-expressing animals. Scale bar is 20 μm in each panel.

Figure 4. The 588 aa fragment of mutant human Htt does not undergo cleavage in *Drosophila*. (A, B) Transient transfection of *Drosophila* S2 cells with eGFP-HttQ15-mRFP (A) or eGFP-HttQ138-mRFP (B) demonstrates no separation of eGFP (green) and mRFP (magenta) signals, suggesting that the mutant Htt protein does not undergo cleavage in S2 cells. (C-E) Visualization of signal localization in 3rd instar larvae with expression of eGFP-HttQ138-mRFP driven by the C155 shows no separation of eGFP (green) and mRFP (magenta) signals in CNS neurons (C), salivary gland cells (D), or epidermal cells (E). (F) Western analysis of brain extracts from control *white* animals, and animals expressing Q138-mRFP or eGFP-Q138-mRFP, showing expression of the Htt protein (asterisk). Immunoblotting with anti-Htt antibodies reveals no differential breakdown product in the double-labeled strain compared to single-labeled lines or control animals that do not express Htt.

Figure 5. Cytoplasmic aggregation of HttQ96-GFP in neuronal and non-neuronal tissues. (A) Visualization of UAS-GFP (green) expression alone in the salivary gland shows localization to the cytoplasm and nucleus (indicated by N). (B) Visualization of HttQ96-GFP (green) in the salivary gland. Unlike GFP, HttQ96-GFP forms cytoplasmic aggregates in the salivary gland. The nucleus is indicated by N, with aggregates indicated by arrowheads. (C, D) Visualization of GFP alone or HttQ96-GFP in CNS neurons of the ventral nerve cord. GFP is diffusely localized in CNS neurons, while HttQ96-GFP forms aggregates. Several Htt aggregates are denoted by arrowheads. (E) HttQ96-GFP aggregates (green, indicated by arrowheads) are found in axons labeled expressing dsRed (magenta) in C155, UAS-dsRed, UAS-HttQ96-GFP larvae. (F) In peripheral axons and synapses of C155, UAS-GFP larvae, GFP (green) is diffuse in the

cytoplasm. (G) In contrast, HttQ96-GFP (green) is found in cytoplasmic aggregates (indicated by arrows) in peripheral axons and synapses in C155, UAS-HttQ96-GFP larvae.

Figure 6. FRAP microscopy shows that mRFP-HttQ138 aggregates continue to accumulate HttQ138 in live anesthetized 3rd instar larval axons. (A) Averaged traces comparing FRAP rates of regions of axons with no aggregates, large aggregates that equal or exceed the diameter of the axon, and smaller aggregates less than the diameter of the axon. While regions without aggregates recover quickly due to fast axonal transport, large and small HttQ138 aggregates recover at a slower rate, but to a greater level. The graph shows percent of initial fluorescence, not total fluorescence. Larger aggregates recover at a greater rate than smaller ones. (B) HttQ138 aggregation kinetics demonstrated by FRAP in different regions of the motor neuron. (C) Time-lapse images of a FRAP experiment showing recovery of an aggregate over 40 minutes in a live anesthetized 3rd instar larval motor neuron axon.

Figure 7. Acute induction of mRFP-HttQ138 expression by *CCAP*-GAL4 shows the pattern of aggregate formation in salivary glands, ventral nerve cord, and axons over 24 hours. Expression of UAS-HttQ138 was repressed using *tubulin*-Gal80^{ts} at 19°C during early development. Animals were moved to 30°C for the designated time, dissected, and imaged immediately to avoid fixation artifacts.

Figure 8. Suppression of lethality with a Df haploinsufficiency screen. (A) Male/female viability ratio of mRFP-HttQ138 expressing Df lines. Homozygous mRFP-HttQ138 females were crossed to C155/y; Df/Bal males for 81 Df lines on chromosome II and 60 Df lines on

chromosome III. Few female escapers expressing mRFP-HttQ138 are ever seen in control crosses (male/female ratio = 0.01). All Dfs with a viability ratio greater that 0.1 were identified as hits. (B-F) Confocal images of mRFP-HttQ138 aggregates in the salivary glands of 3rd instar larvae from controls (B) and animals heterozygous for *Df(3L)vin7* (C), *Df(2R)sple-J1* (D), *Df(2R)AA21* (E) and *Df(2R)59AB* (F). The scale bar is 100 μm in all panels.

Figure 9. Quantification of transgenic Htt expression. (A) Western blot with C155-driven HttQ138 expression in control (white) and the indicated genotypes from pupal head extracts probed with anti-Htt antibodies and control anti-actin antibodies. (B) Quantification of C155-driven HttQ138 protein expression in control (white) and the indicated genotypes from pupal head extracts. The control containing C155; UAS-mRFP-HttQ138 was normalized to one for the genotypic comparisons. (C) Quantification of C155-driven GFP-CD8 expression in control (white) and the indicated genotypes from adult head extracts by Western blot analysis with anti-GFP antibodies. (D) HttQ138 mRNA levels were measured in pupal head extracts by quantitative RT-PCR and normalized to control (white) expression. Error bars indicate SEM. * indicates $p<0.05$ by Student's t-test.

Figure 10. HttQ138 and Synaptotagmin aggregation in peripheral axons. Confocal images of 3rd instar larval peripheral nerves expressing mRFP-HttQ138 (red-left panel) and immunostained with anti-synaptotagmin I antibodies (green- middle panel) from controls (A) and animals heterozygous for PBc02324 (B), *lab*^{14} (C), *Df(3L)vin7* (D), *Df(2R)sple-J1* (E), *Df(2R)AA21* (F) and *Df(2R)59AB* (G). The scale bar is 10 μm for all panels. (H) Quantification of HttQ138 aggregate number for 100 μm axon segments for 25 segments (n= 5 larvae) of the indicated

genotypes. Aggregates > 0.5 μm were counted using the 'find 2D nucleus' function of the Velocity version 5.4 software (Perkin Elmer). Error bars indicate SEM, with * denoting $p<0.05$ using Student's t-test.

Figure 11. Graph of lifespan versus soluble HttQ138 (measured by Western blot) or axonal aggregates (quantified per 100 μm section of larval axon) for identified suppressors. Htt expression and aggregation are tightly linked and correlate with increased toxicity. *Df(2R)sple-J1* has reduced toxicity that is correlated with decreased soluble Htt only.

Supplemental Figure 1. Fine mapping for two genetic intervals uncovered in the initial suppressor screen for HttQ138 pupal lethality. (A) Suppressors *Df(3L)st-f13* (Bloomington stock 2993) and *Df(3L)brm11* (Bloomington stock 3640) overlap the 72C1-72D5 interval. Mapping with additional aberrations contained within the Bloomington Stock Center demonstrated that stock 10887 (PBc02324) rescued HttQ138 expressing animals at 15% of expected viability. (B) Suppressor *Df(3R)Tpl10* (Bloomington stock 1990) was sub-mapped to a single genetic aberration within the region defined by stock 2092 (lab^{14}) that increased the expected adult viability ratio to 24%.

Supplemental Figure 2. Quantitative RT-PCR was performed on the PBc02324 p-element insertion mutant. The transcript levels of both genes surrounding the insertion, CG5830 and *mRpS31*, were measured in homozygous mutant heads compared to white flies. Both genes appear slightly downregulated in the mutant, but only CG5830 was statistically significant. Error bars indicate SEM, with * denoting $p<0.05$ using Student's t-test.

Supplemental Table 1. Table showing the 166 Bloomington deficiency kit strains that were tested in the initial screen, along with the number of viable flies and changes in salivary gland aggregation. The viability data is represented graphically in figure 8A.

Supplemental Table 2. Table showing stocks used for mapping of screen hits**.** Control data is listed on the first page. Each additional page heading represents mapping from the original large Df identified in the screen. The cells within each page list most of the smaller deficiencies tested in each region and their results for viability and/or aggregation where applicable.

Supplemental Video 1. Time-lapse confocal images of *CCAP*-GAL4; mRFP-HttQ138 showing FRAP of four aggregates of various sizes. Frame rate is 1 per 60 seconds for a total time of 60 minutes.

Figure 1

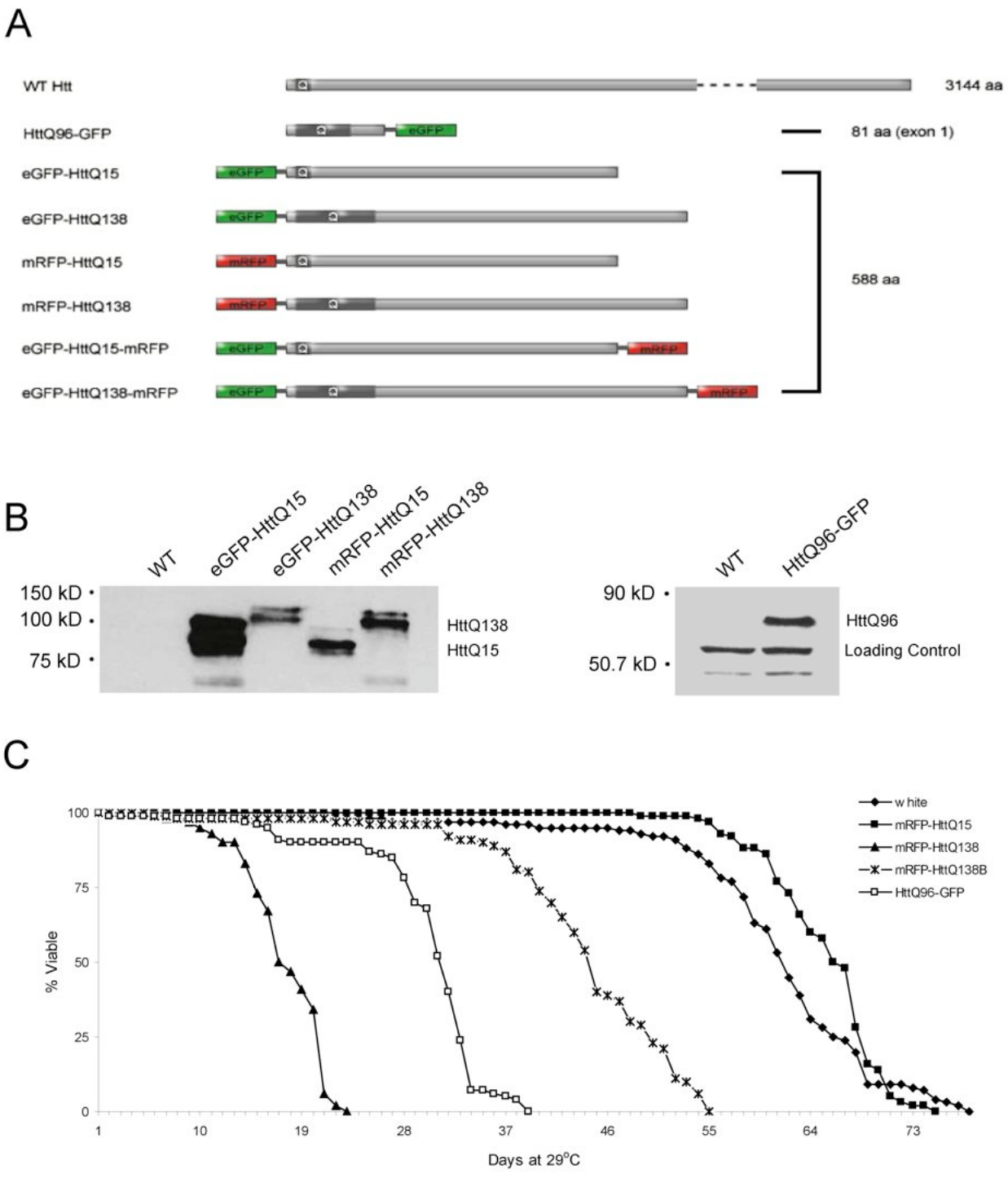
A
WT Htt
3144 aa
HttQ96-GFP
eGFP
81 aa (exon 1)
eGFP-HttQ15
eGFP-HttQ138
mRFP-HttQ15
mRFP-HttQ138
eGFP-HttQ15-mRFP
eGFP-HttQ138-mRFP
mRFP
588 aa
B
WT
eGFP-HttQ15
eGFP-HttQ138
mRFP-HttQ15
mRFP-HttQ138
150 kD
100 kD
75 kD
HttQ138
HttQ15
WT
HttQ96-GFP
90 kD
50.7 kD
HttQ96
Loading Control
C
% Viable
Days at 29°C
w hite
mRFP-HttQ15
mRFP-HttQ138
mRFP-HttQ138B
HttQ96-GFP

Figure 2

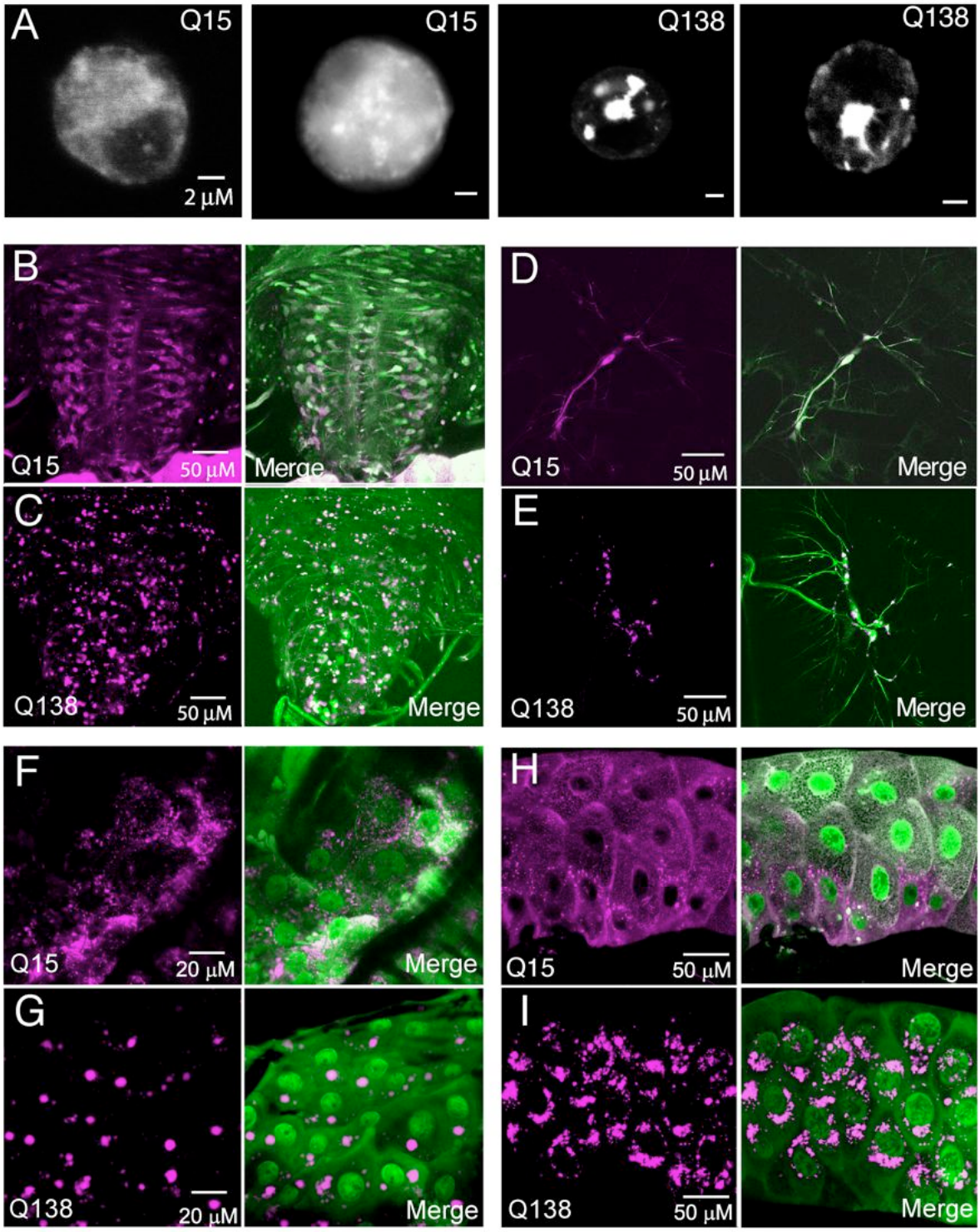
A
Q15
2 μM
Q15
Q138
Q138
B
Q15
50 μM
Merge
D
Q15
50 μM
Merge
C
Q138
50 μM
Merge
E
Q138
50 μM
Merge
F
Q15
20 μM
Merge
H
Q15
50 μM
Merge
G
Q138
20 μM
Merge
I
Q138
50 μM
Merge

Figure 3

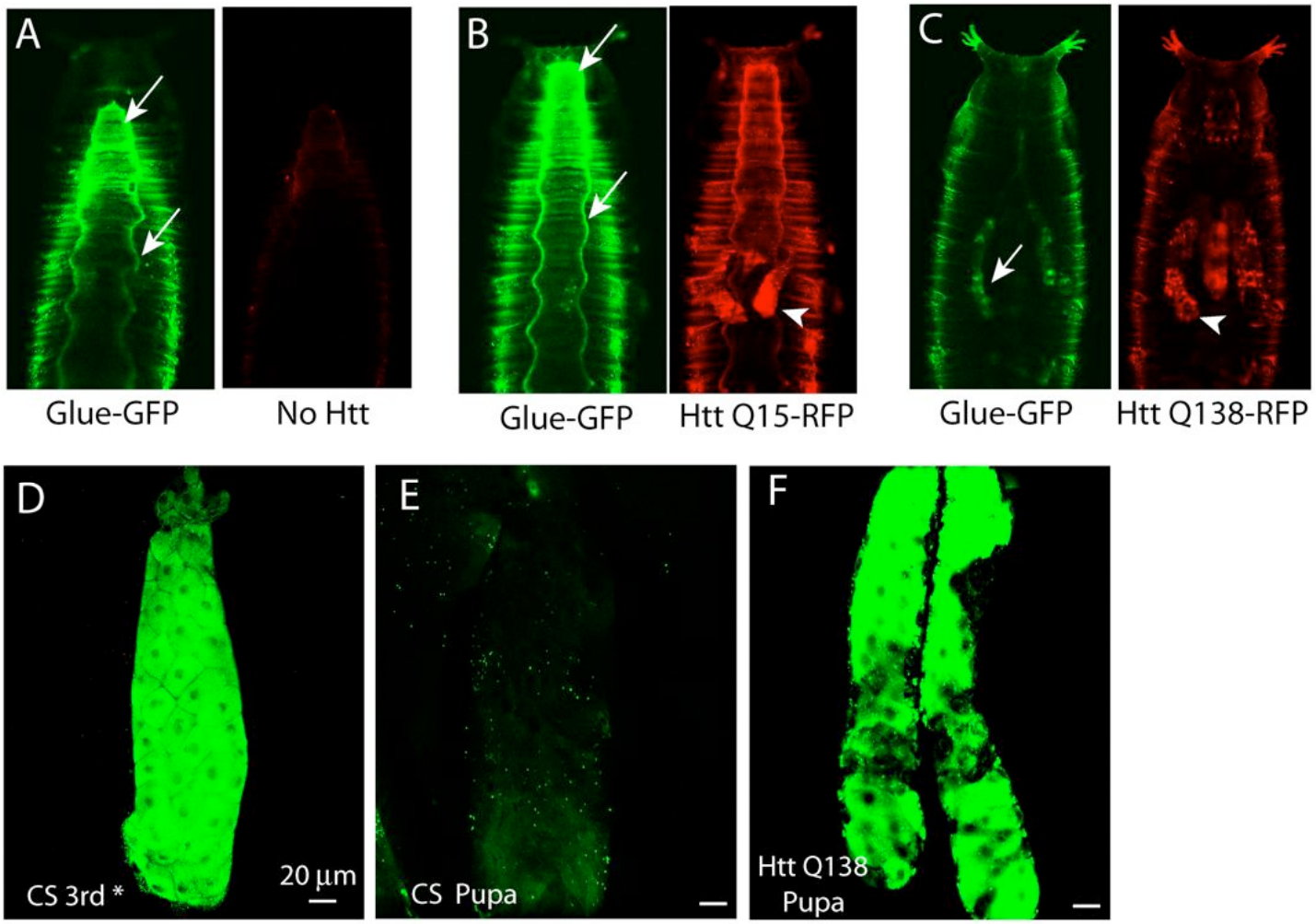
A
Glue-GFP
No Htt
B
Glue-GFP
Htt Q15-RFP
C
Glue-GFP
Htt Q138-RFP
D
CS 3rd *
20 µm
E
CS Pupa
F
Htt Q138
Pupa

Figure 4

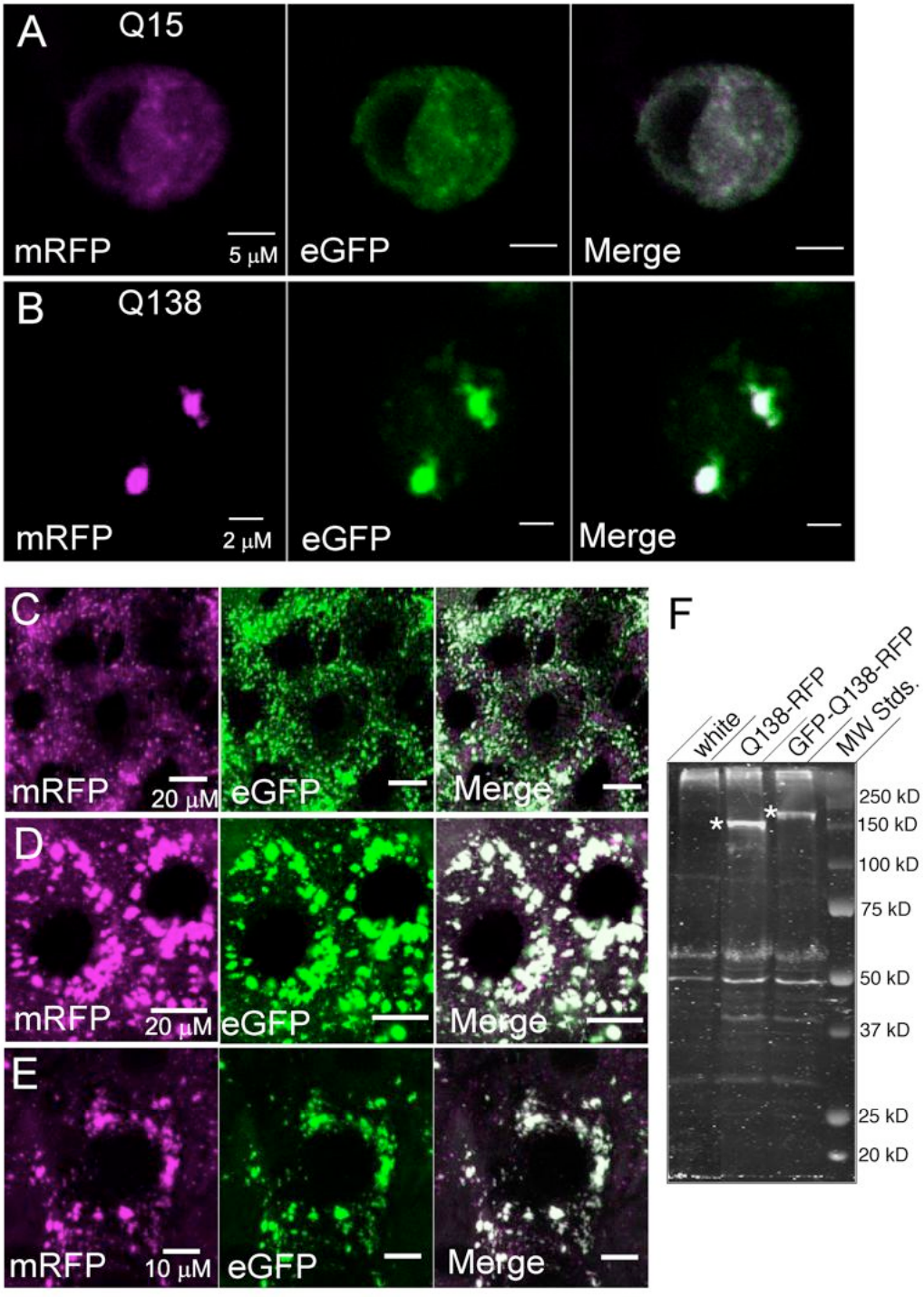
A
Q15
mRFP
5 μM
eGFP
Merge
B
Q138
mRFP
2 μM
eGFP
Merge
C
mRFP
20 μM
eGFP
Merge
D
mRFP
20 μM
eGFP
Merge
E
mRFP
10 μM
eGFP
Merge
F
white
Q138-RFP
GFP-Q138-RFP
MW Stds.
250 kD
150 kD
100 kD
75 kD
50 kD
37 kD
25 kD
20 kD

Figure 5

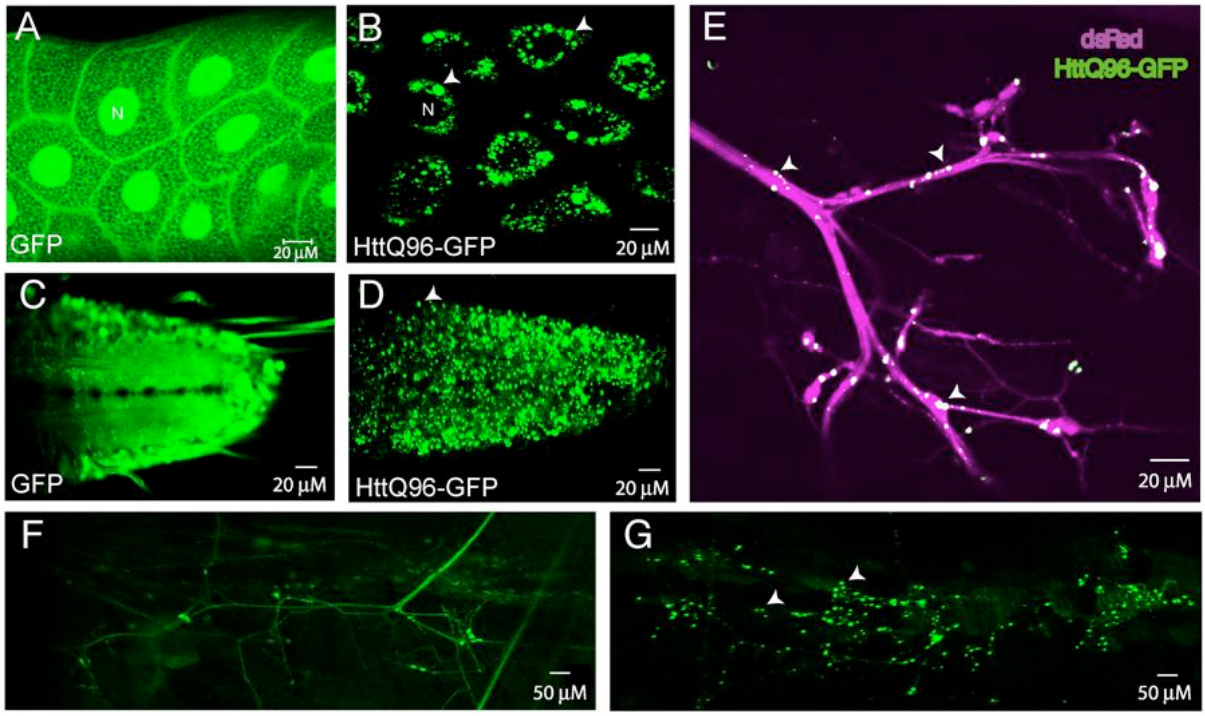
A
N
GFP
20 µM
B
N
HttQ96-GFP
20 µM
E
dsRed
HttQ96-GFP
20 µM
C
GFP
20 µM
D
HttQ96-GFP
20 µM
F
50 µM
G
50 µM

Figure 6

A

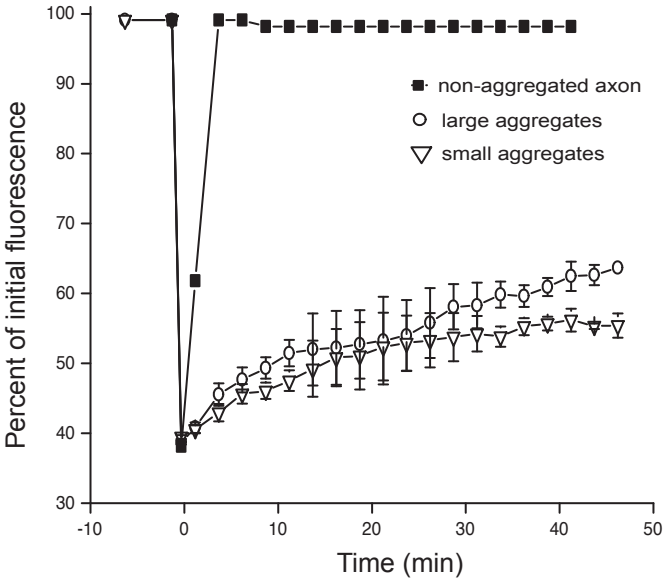
Percent of initial fluorescence
Time (min)
non-aggregated axon
large aggregates
small aggregates

B

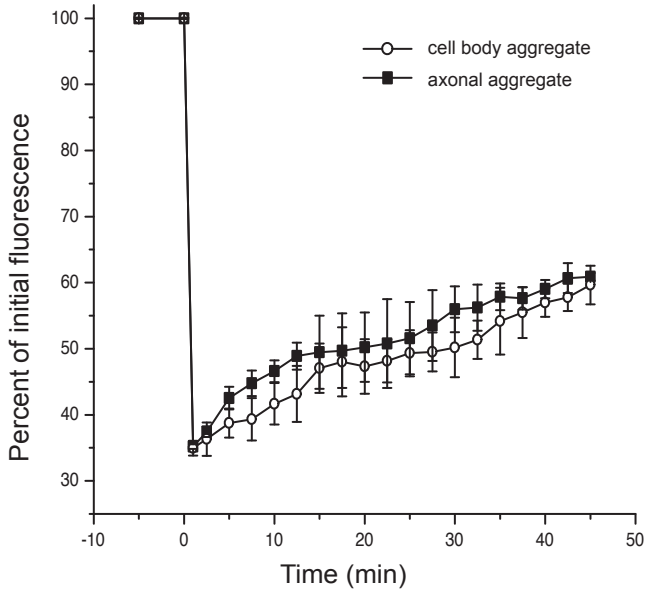
Percent of initial fluorescence
Time (min)
cell body aggregate
axonal aggregate

C

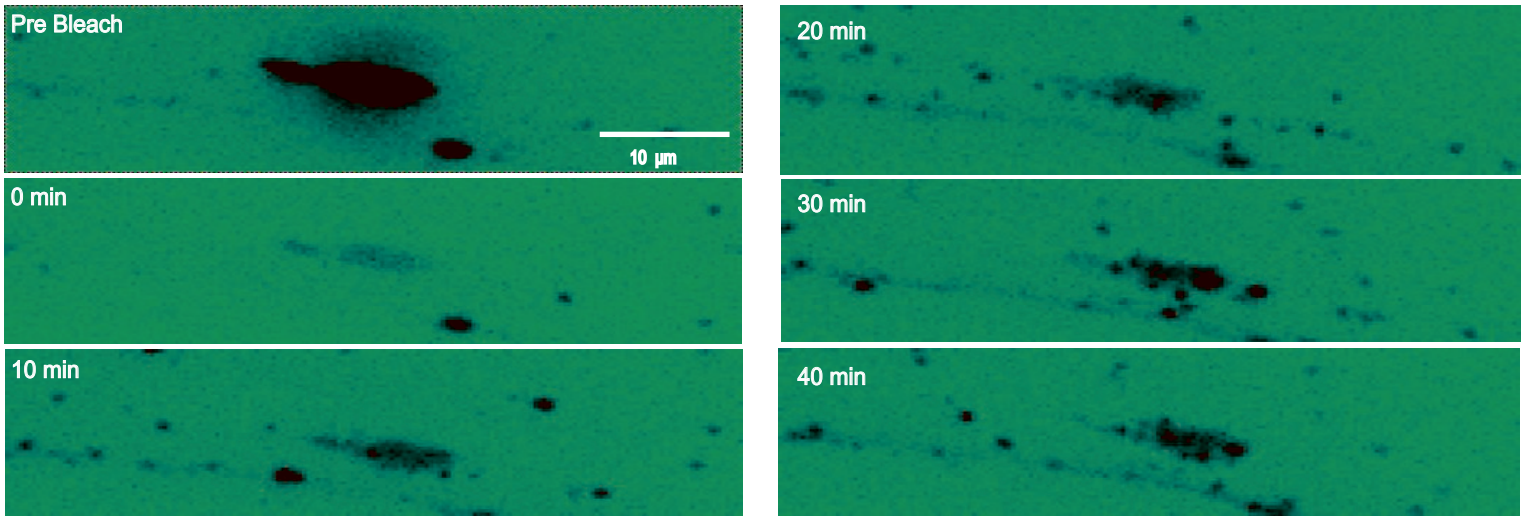
Pre Bleach
10 µm
0 min
10 min
20 min
30 min
40 min

Figure 7

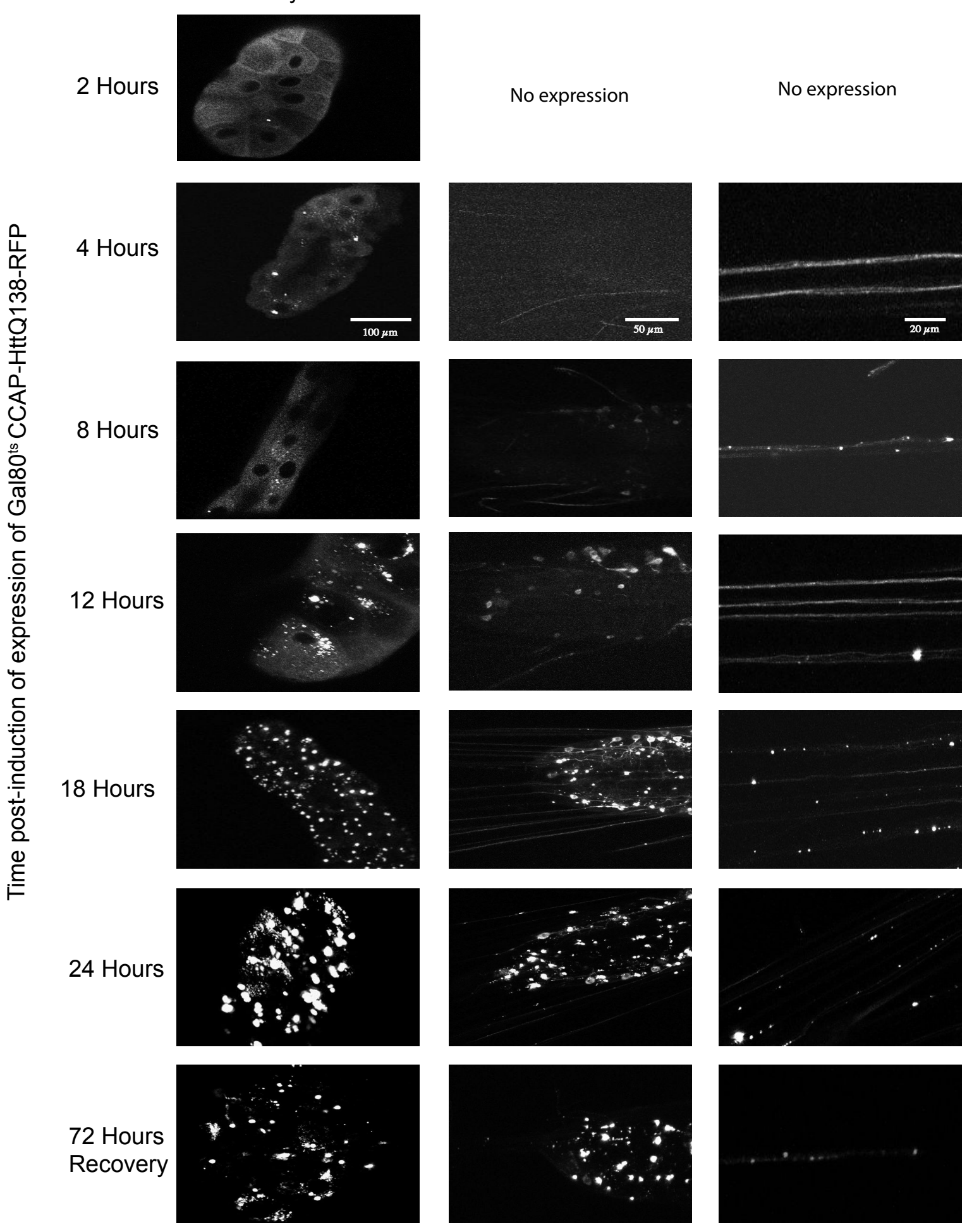
Salivary Gland
Ventral Nerve Cord
Axons
2 Hours
No expression
No expression
4 Hours
100 μm
50 μm
20 μm
8 Hours
12 Hours
18 Hours
24 Hours
72 Hours Recovery
Time post-induction of expression of Gal80ts CCAP-HttQ138-RFP

Figure 8

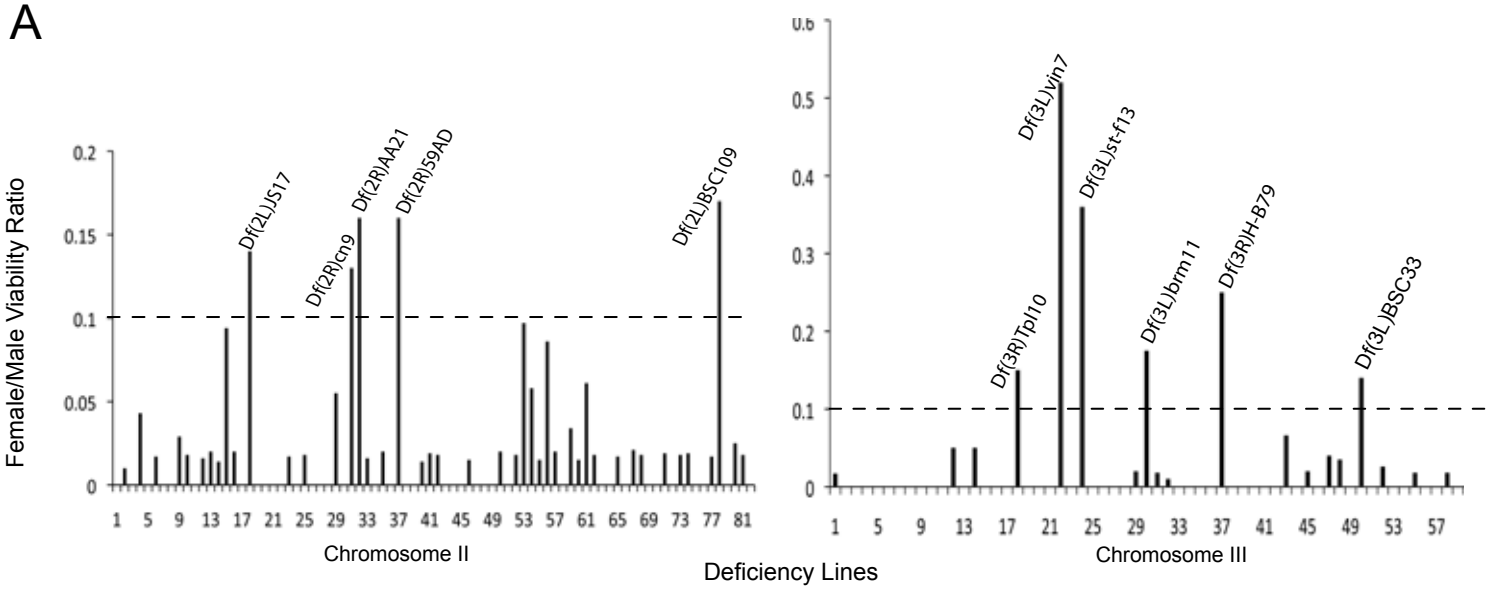
A
Female/Male Viability Ratio
0.2
0.15
0.1
0.05
0
Df(2L)JS17
Df(2R)cn9
Df(2R)AA21
Df(2R)59AD
Df(2L)BSC109
1 5 9 13 17 21 25 29 33 37 41 45 49 53 57 61 65 69 73 77 81
Chromosome II
0.6
0.5
0.4
0.3
0.2
0.1
0
Df(3L)vin7
Df(3L)st-f13
Df(3R)Tpl10
Df(3L)brm11
Df(3R)H-B79
Df(3L)BSC33
1 5 9 13 17 21 25 29 33 37 41 45 49 53 57
Chromosome III
Deficiency Lines

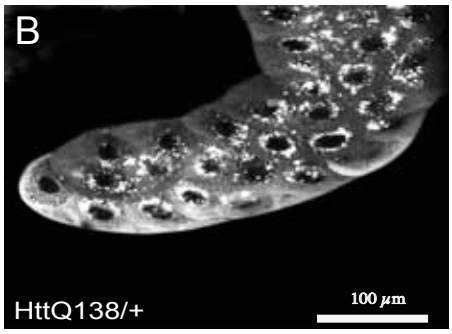
B
HttQ138/+
100 μm

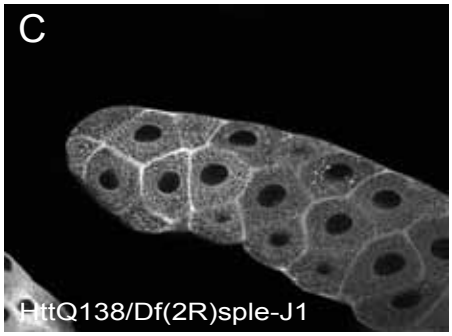
C
HttQ138/Df(2R)sple-J1

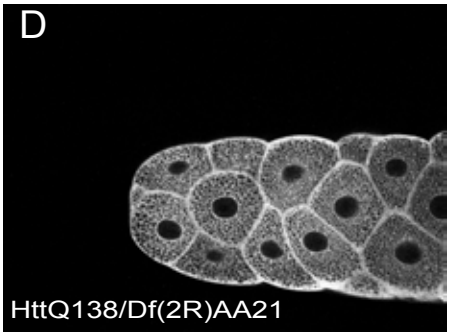
D
HttQ138/Df(2R)AA21

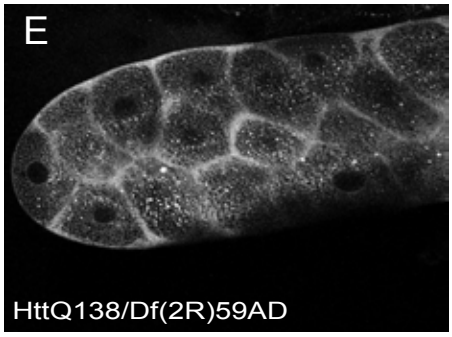
E
HttQ138/Df(2R)59AD

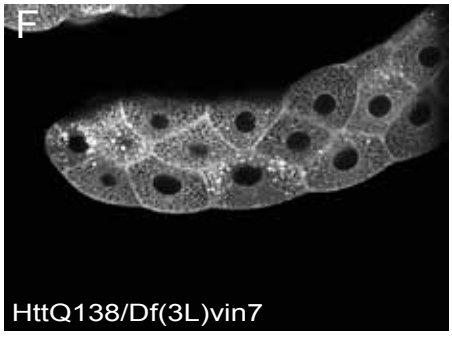
F
HttQ138/Df(3L)vin7

Figure 9

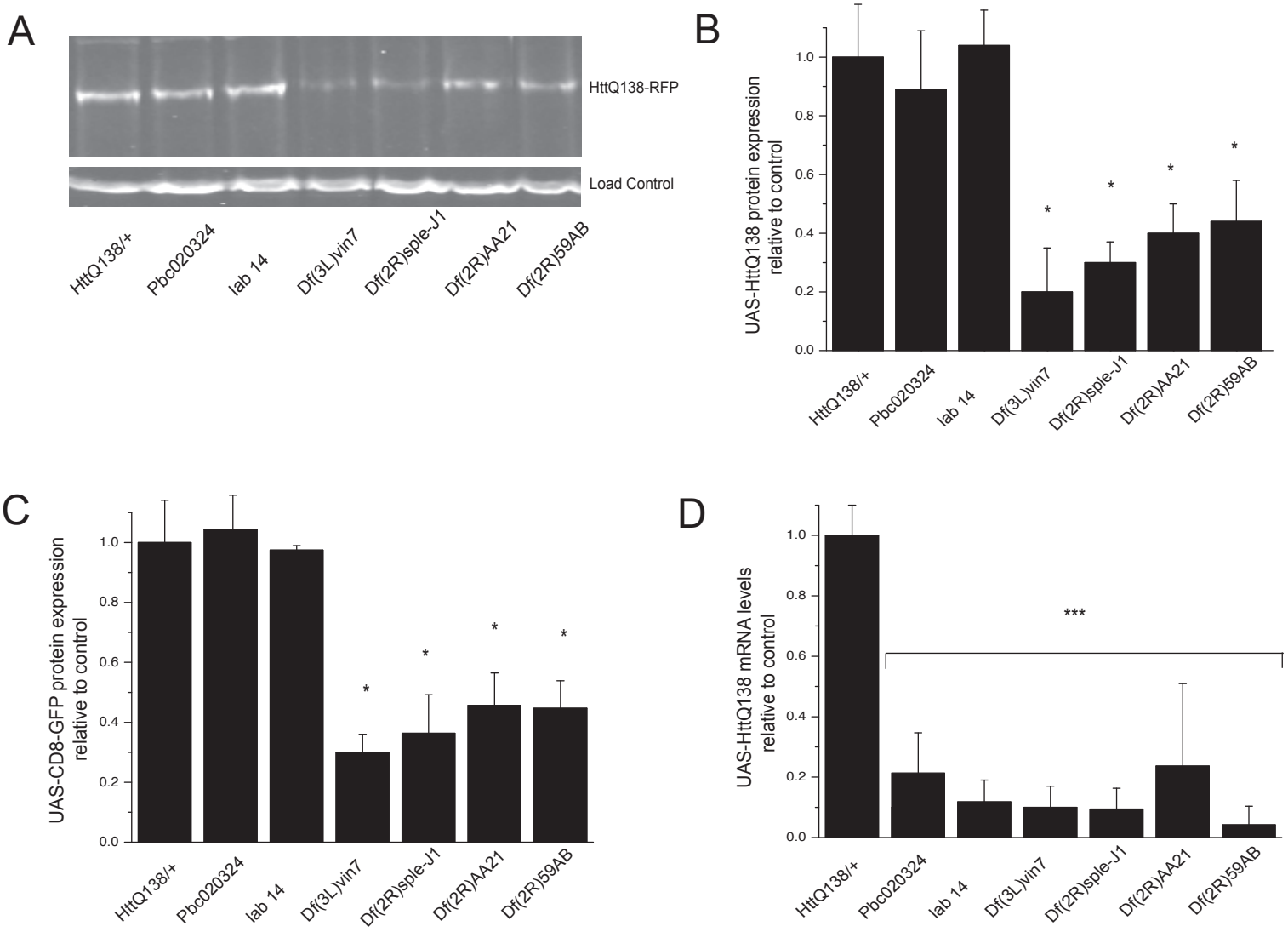
A
HttQ138-RFP
Load Control
HttQ138/+
Pbc020324
lab 14
Df(3L)vin7
Df(2R)sple-J1
Df(2R)AA21
Df(2R)59AB
B
UAS-HttQ138 protein expression relative to control
0.0
0.2
0.4
0.6
0.8
1.0
*
C
UAS-CD8-GFP protein expression relative to control
D
UAS-HttQ138 mRNA levels relative to control
***

Figure 10

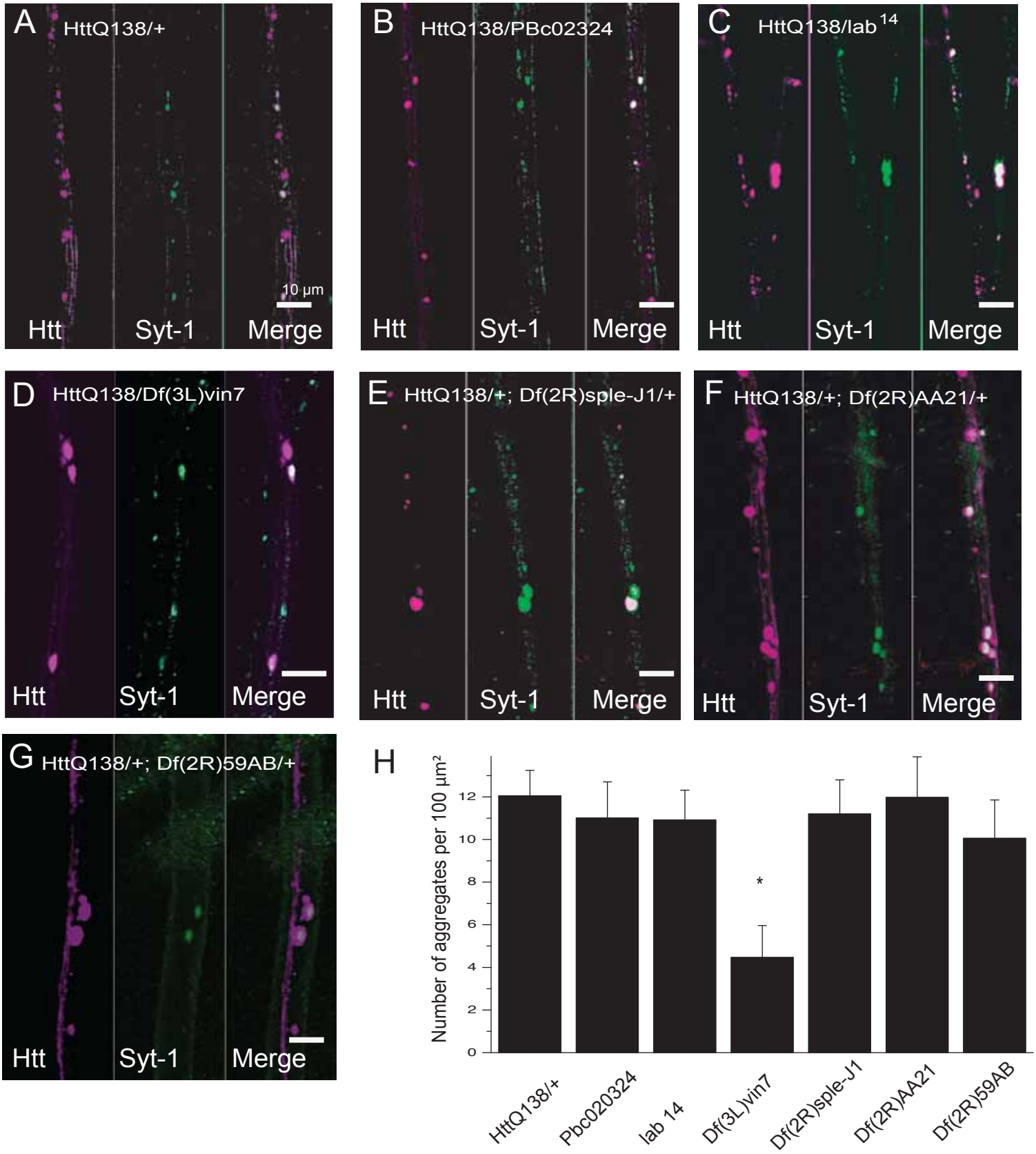
A HttQ138/+
10 µm
Htt
Syt-1
Merge
B HttQ138/PBc02324
Htt
Syt-1
Merge
C HttQ138/lab 14
Htt
Syt-1
Merge
D HttQ138/Df(3L)vin7
Htt
Syt-1
Merge
E HttQ138/+; Df(2R)sple-J1/+
Htt
Syt-1
Merge
F HttQ138/+; Df(2R)AA21/+
Htt
Syt-1
Merge
G HttQ138/+; Df(2R)59AB/+
Htt
Syt-1
Merge
H
Number of aggregates per 100 µm²
0
2
4
6
8
10
12
*
HttQ138/+
Pbc020324
lab 14
Df(3L)vin7
Df(2R)sple-J1
Df(2R)AA21
Df(2R)59AB

Figure 11

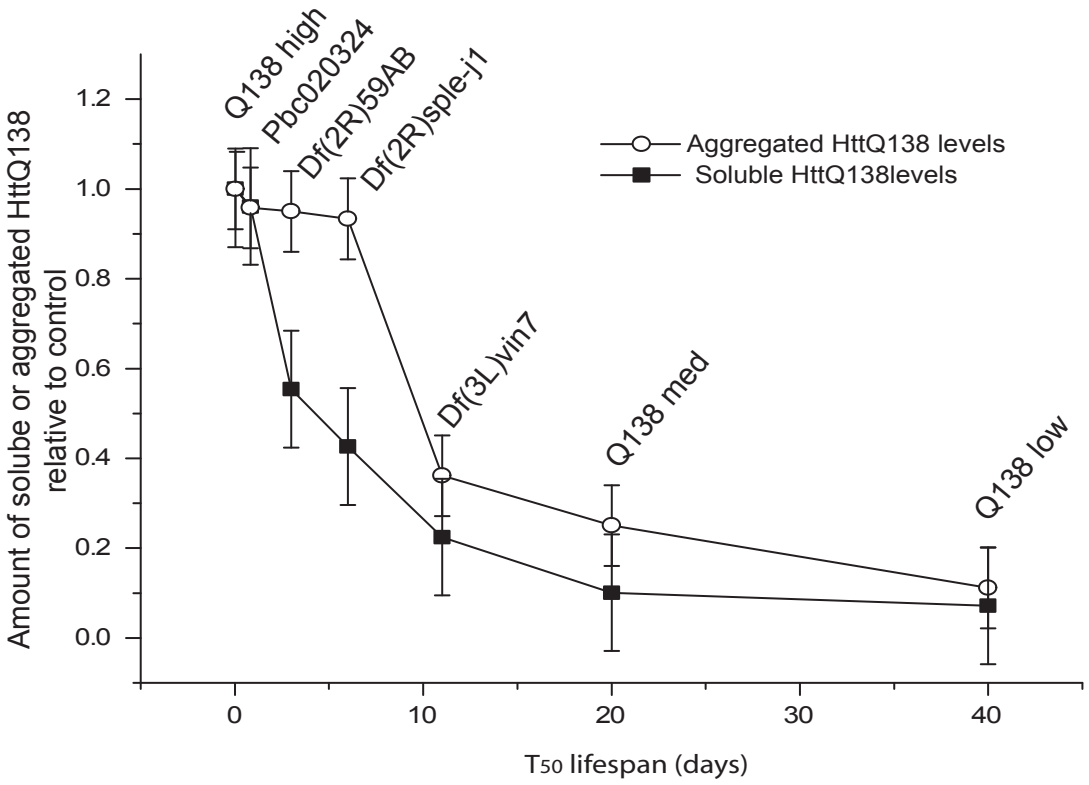
Q138 high
Pbc020324
Df(2R)59AB
Df(2R)sple-j1
Df(3L)vin7
Q138 med
Q138 low
Aggregated HttQ138 levels
Soluble HttQ138levels
Amount of solube or aggregated HttQ138 relative to control
1.2
1.0
0.8
0.6
0.4
0.2
0.0
0
10
20
30
40
T50 lifespan (days)

Supplemental Figure 1

A

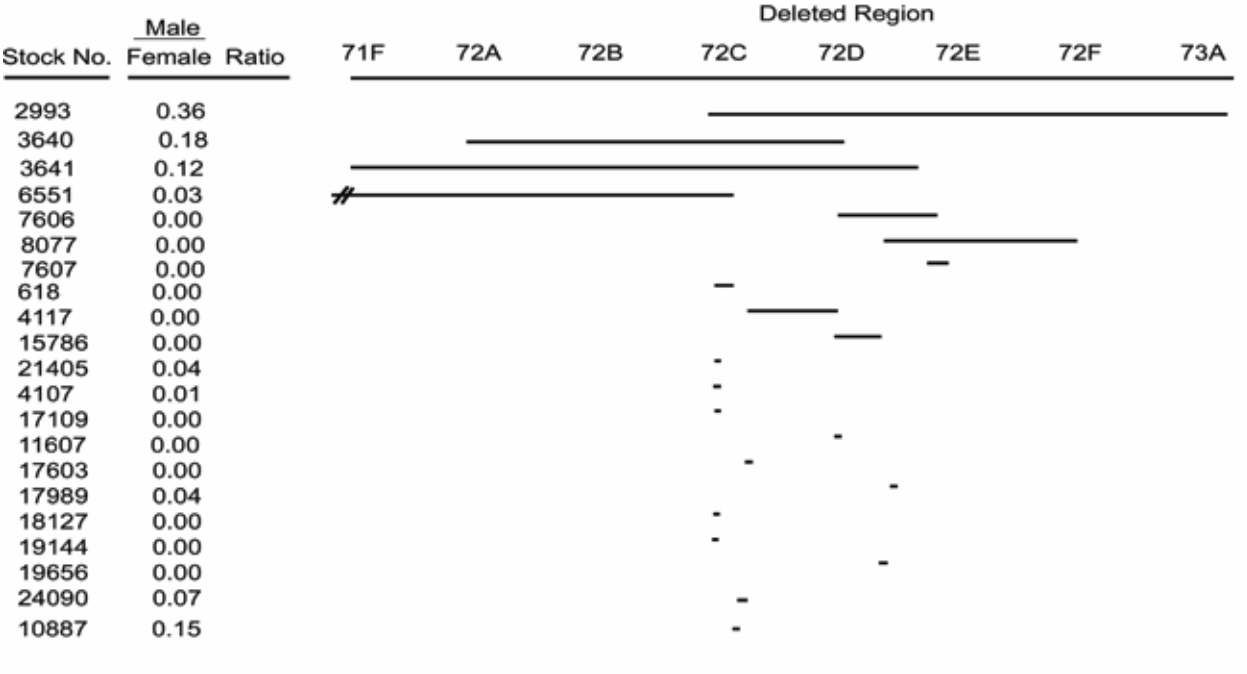

B

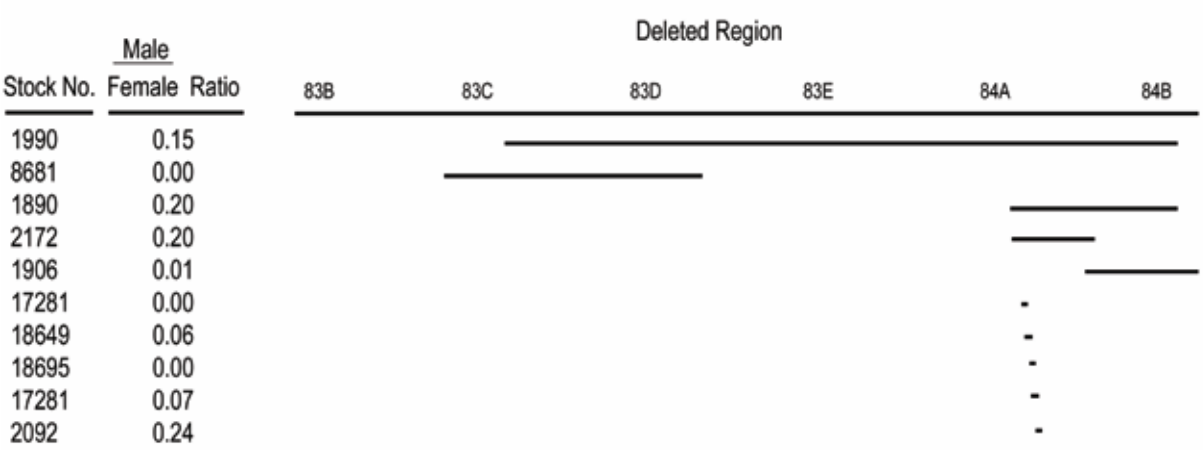

Supplemental Figure 2